The P-wave Boundary of the Large-Low Shear Velocity Province beneath the Pacific

Daniel A. Frost, Sebastian Rost

March 2014

1 Abstract

The Large Low Shear Velocity Provinces (LLSVPs) in the lower mantle represent volumetrically significant thermal or chemical or thermo-chemical heterogeneities. Their structure and boundaries have been widely studied, mainly using S-waves, but much less is known about their signature in the P-wavefield. We use an extensive dataset recorded at USArray to create, for the first time, a high-resolution map of the location, shape, sharpness, and extent of the boundary of the Pacific LLSVP using P(P_{diff})-waves. We find that the northern edge of the Pacific LLSVP is shallow dipping (26 to 32° relative to the horizontal) and diffuse (~120 km wide transition zone) whereas the eastern edge is steeper dipping (60°) and apparently sharp (~60 km wide). We trace the LLSVP boundary up to ~500 km above the CMB in most areas, and 700 km between 120 and 90° W at the eastern extent of the boundary. Apparent P-wave velocity drops are ~1-3 % relative to PREM, indicating a strong influence of LLSVPs on P-wave velocity, at least in the high-frequency wavefield, in contrast to previous studies. Localised patches with greater velocity drops are detected, defined by high travel-time gradients. We identify these as a likely location of an Ultra-Low Velocity Zones (ULVZs), matching the location of a previously detected ULVZ in this area. The boundary of a separate low velocity anomaly, of a similar height to the LLSVP, is detected in the north-west Pacific, matching tomographic images. This outlier appears to be connected to the main LLSVP through a narrow channel close to the CMB and may be in the process of joining or splitting from the main LLSVP. We also see strong velocity increases in the lower mantle to the east of the LLSVP, likely detecting subducted material beneath central America. The LLSVP P-wave

boundary is similar to that determined in high-resolution S-wave studies and follows the -0.4 % ΔV_S iso-velocity contour in the S40RTS tomography model. Additionally, the LLSVP boundary roughly matches the shape of the -0.4 % ΔV_P iso-velocity contour but defines an area more similar to that defined by the 0.0 % V_P iso-velocity contour of the P-wave model GyPSuM. High resolution P-wave velocity determination allows for estimation of the ratio of P- and S-wave velocity anomalies ($R_{S,P}$) which can be used to indicate dominantly thermal or chemical control of seismic velocities. Our observations of the Pacific LLSVP are consistent with a thermo-chemical anomaly whose shape and boundary sharpness are controlled by proximity to active and past subduction.

Keywords

P-waves; LLSVP; Deep Earth Seismology; Lower Mantle; Seismic Body-waves; USArray

2 Introduction

Tomographic S-wave images of the lowermost mantle are dominated by two nearly antipodal volumes of strongly reduced seismic S-wave velocity [e.g. Dziewonski, 1984, Ritsema et al., 1999, Panning and Romanowicz, 2006, Simmons et al., 2010, Ritsema et al., 2011, Lay and Garnero, 2011]. These structures are commonly referred to as Large-Low Shear Velocity Provinces (LLSVP) and are characterised by a shear-wave (S-wave) velocity drop of about 2% in tomography models and 3-5% in high-resolution S-wave studies [Ritsema et al., 1997, 1998, Ni and Helmberger, 2003b, Wang and Wen, 2007, Lay and Garnero, 2011] relative to 1D Earth models [e.g. Dziewonski and Anderson, 1981, Kennett and Engdahl, 1991] extending from the Core Mantle Boundary (CMB) to ~1000 km above [Burke et al., 2008, Helmberger et al., 2009]. Other geophysical evidence points to an increased density within the LLSVPs [Ishii and Tromp, 1999]. The structure and location of the LLSVPs is very consistent between different tomographic S-wave models [Lekic et al., 2012] but is less well constrained for P-waves. The LLSVPs might have an influence on surface tectonics with hotspot volcanism showing a strong correlation with the edges of the LLSVPs [Williams et al., 1998, Thorne et al., 2004], as do the palaeo-locations of Large Igneous Provinces (LIPS) [Torsvik et al., 2006], and geochemical anomalies [Dupre and Allegre, 1983, Hart, 1984, Castillo, 1988]. LLSVPs are also suggested to influence the pattern of outer core convection, thereby modifying the generation of the Earth's magnetic field [Gubbins et al., 2007, Davies et al., 2008]. Both S- and P-wave tomographic images indicate that the LLSVPs are surrounded by high seismic velocities relative to 1D models which have been related to pooling of subducted slabs, described as "slab graveyards"

[Richards and Engebretson, 1992, Garnero and Helmberger, 1995]. This is supported by seismic evidence showing the strongest seismic velocity gradients at the edges of these structures [Thorne et al., 2004] and sharp boundaries to the LLSVPs (resolved only with S-waves) [Ritsema et al., 1997, 1998, Ni et al., 2002, Ni and Helmberger, 2003a, Wang and Wen, 2004, Helmberger and Ni, 2005, To et al., 2005, Ford et al., 2006, Wang and Wen, 2007, He and Wen, 2012]. LLSVPs might be related to smaller-scale lowermost mantle structures such as ultra-low velocity zones (ULVZs) [Garnero and Helmberger, 1995, Rost and Garnero, 2004, Rost et al., 2005, Lay et al., 2006] and compositional heterogeneities [Hedlin and Shearer, 2000, Frost et al., 2013], through internal mixing and settling of denser material [McNamara et al., 2010]. One of the enigmatic features of LLSVPs is the apparent anti-correlation between S-wave and bulk-sound speed, as resolved in global tomographic images [Masters et al., 2000]. This combination of geophysical observations led to a model of the LLSVPs as dense thermo-chemical piles [McNamara and Zhong, 2005], although purely thermal models of LLSVPs have also been discussed [Schuberth et al., 2009, Davies et al., 2012].

Within the mineralogy of mantle materials, the transition from perovskite to post-perovskite under lower mantle pressures is calculated to be sensitive to temperature, primarily occuring in relatively cold conditions, such as regions related to subduction [Murakami et al., 2004, Oganov and Ono, 2004]. The sharp velocity increase with depth resulting from the transition to post-perovskite has been discussed as the source of the D$''$ reflector [Murakami et al., 2004, Oganov and Ono, 2004]. The apparent absence of the D$''$ reflector within LLSVPs implies that LLSVPs are likely hotter than the surrounding mantle, where the D$''$ reflector is more commonly seen [Thomas et al., 2004, Hutko et al., 2009].

Geodynamic models of dense thermo-chemical piles indicate that the location of LLSVPs can be explained well by material slightly denser than the surrounding mantle. Some models require density and bulk-modulus increases of $\sim$2 and $\sim$7 %, respectively, to maintain the anomaly shape [Tan and Gurnis, 2005, 2007]. In other studies, a density increase of 2 to 5% seems sufficient to avoid entrainment of the material in mantle flow [McNamara and Zhong, 2005, Garnero and McNamara, 2008] and allows stable piles over the lifetime of the Earth. In these models the dense material is swept into approximately the correct location and shape in the lower mantle if constraints of the recent to present subduction history are taken into account [McNamara and Zhong, 2005]. The roughly antipodal location of the LLSVPs along the equator can, therefore, be linked to the orientation of the Earth's rotation axis [Richards et al., 1997, Steinberger and Torsvik, 2008]. The location of the LLSVPs seems to be a consequence of the overall dynamics of the Earth's mantle [Trønnes, 2010].

The origin of the LLSVPs is widely debated with models that can be roughly divided into those requiring accumulation of primordial material through incomplete segregation of the mantle [Becker et al., 1999, Labrosse et al., 2007], and those where LLSVPs are built up by the segregation of subduction products (i.e. the deposition of mid-oceanic ridge basalts (MORB)) [Christensen and Hofmann, 1994, Brandenburg and van Keken, 2007, van Keken et al., 2010]. Segregation of MORB as a source for lower mantle heterogeneities would be a continuous process [Christensen and Hofmann, 1994], while isotope studies require an untapped primordial reservoir that might have been formed as early as 400 to 500 Myr into Earth's history [Boyet and Carlson, 2005, Carlson and Boyet, 2006]. Recent combined geodynamical, seismological and mineral physics studies indicate that it might be difficult to fit the geophysical characteristics of LLSVPs by MORB accumulation [Deschamps et al., 2012, Li and McNamara, 2013].

The location of LLSVPs at the CMB is well resolved using S-wave tomographic techniques [Lekic et al., 2012], although resolution of the precise boundaries is poor close to the CMB [Panning and Romanowicz, 2006, Lay and Garnero, 2011], which, instead, can be determined with high-resolution travel-time and waveform studies [To et al., 2005, Ford et al., 2006, He and Wen, 2009, 2012]. Nonetheless, the shape of the LLSVPs above the D$''$ region is less well resolved due to a decay of resolution in tomographic images. Despite wide ranging agreement for S-waves, P-wave tomography models fail to agree on the location of the LLSVPs, and no attempt has been made for a high resolution determination of the boundaries of the Pacific LLSVP using P-wave travel times and waveforms as has been done with S-waves [He and Wen, 2012]. Indeed, P-wave studies report little to no response to the African LLSVP structure from P-waves in terms of either travel-times or waveforms [Helmberger and Ni, 2005].

The location of the boundary and, especially, the steepness of the edges can inform about the viscosity of the LLSVP material and the convective support of the structure [Tan and Gurnis, 2005, McNamara and Zhong, 2005, Tan and Gurnis, 2007]. Furthermore, a comparison between P- and S-wave structure will allow better differentiation between thermal and thermo-chemical models of LLSVPs [Robertson and Woodhouse, 1996a,b, Karato, 2003]. To this end, we attempt to resolve the detailed location of the Pacific LLSVP (despite working with P-waves we will continue to use the term LLSVP to refer to the, possibly dense, thermo-chemical pile beneath the Pacific). Using the lateral extent of USArray [Meltzer et al., 1999] we are able to map the precise location of the Pacific LLSVP, especially in the north and east of the LLSVP. We use travel-times of lower mantle turning and core-grazing P-waves to determine the LLSVP boundary location. We utilise a wide range of epicentral distances and back azimuths to track the vertical and lateral extent of the LLSVP, respectively. We correct for both upper mantle (down to depths of 1600 km) and crustal structure in the receiver region using the combined P-wave geodynamic tomography model GyPSuM [Simmons et al., 2010] and the crustal structure model Crust1.0 [Laske et al., 2012]. We are able to resolve the P-wave boundary of the LLSVP as the transition from positive to negative travel time anomalies. The observed boundary tracks the 0% contour of GyPSuM well, but only partially agrees with the S-wave velocity structure.

3 Method

We employ data from USArray, mainly the Transportable Array (TA) with additional permanent "backbone" stations. USArray has an approximate station spacing of 70 km and is deployed on a grid system (Figure 1). The array has been operational between 2004 and 2014, moving across the USA with stations being relocated roughly every two years. At any one time, there have had between 300 and 600 operating stations. Using this network configuration allows for a wide sampling of the lowermost mantle, both laterally and vertically, due to the large distance and azimuth range covered by the stations.

We search the Reviewed Events Bulletin (REB) catalogue for events with magnitudes of 5.0 and above and select those that have distances from $\sim 85°$ to $\sim 95°$ from the centre-point of the array. We concentrate on events from the Indonesian Arc, Tonga Trench, south-eastern Pacific, and South-American Trench. The great-circle paths of these events to USArray are best suited to sample the northern and eastern edges of the Pacific LLSVP. Although events at any depth, including crustal events, are used in areas with low seismicity, we preferentially use events with depths ≥ 30 km due to their simpler source mechanisms and to reduce travel-time anomalies from crustal and uppermost mantle heterogeneities in the source region. The selected events and stations are shown in Figure 1.

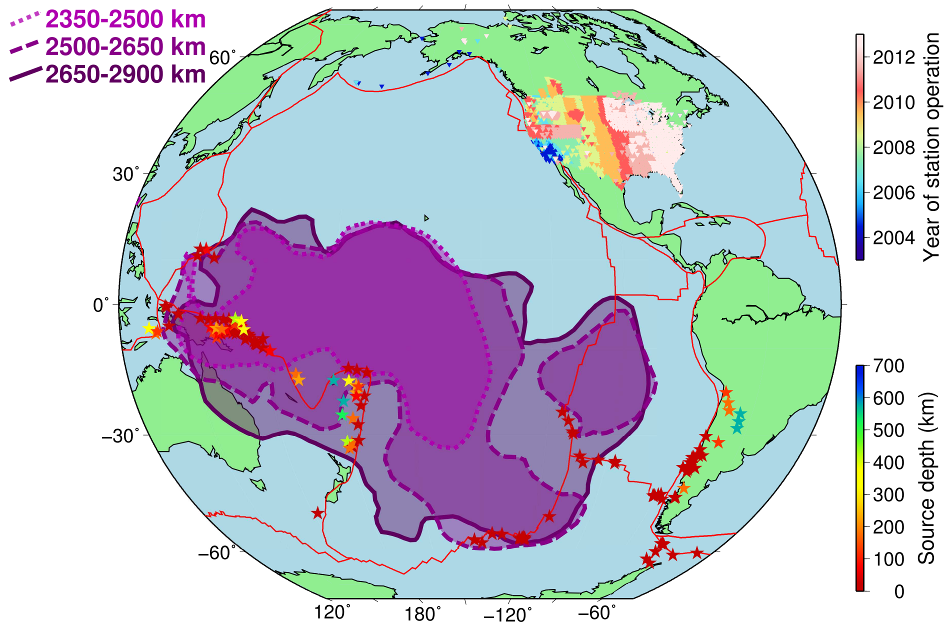

Figure 1: Events and stations used in this study. Events are denoted as stars with colour indicating source depth. A full listing of earthquakes used is shown in the supplementary material (Supplementary Table 1). Stations are shown as inverted triangles with colour indicating year of deployment. Plate boundaries (red lines) from NUVEL-1 [DeMets et al., 1990] are shown along with the area covered by the Pacific LLSVP, as defined by the -0.4 % V_P contour in GyPSuM [Simmons et al., 2010], shown as the purple contours and shaded areas. The LLSVP contours are drawn at 2350-2500 km depth, 2500-2650 km, and 2650-2900 km, as defined by the depth slices in the tomography model. [Span 2 columns]

For each event, data are de-spiked, re-sampled at 40 samples/s, and bandpass filtered. We filter between 0.5 and 1.6 Hz, order 2, as this was found to be best to extract P and P_{diff} arrivals from the noise, where the order controls the rate of decay of energy with frequencies outside of the pass-band. Noisier events, where the P-wave is less clear relative to the noise, are filtered with order 3 or 4, defining a sharper frequency cut-off. To retain as much waveform information as possible, we use the lowest possible order filter that clearly reveals the first arrivals. We only consider traces at distances between 60 and 120° to observe energy turning in the lower mantle. We then visually inspect each trace to decide whether to include it in further processing, based on the P-wave arrival being obvious above the noise.

We apply an adaptive stacking routine [Rawlinson and Kennett, 2004] to find the best alignment of an ensemble of network stations and to determine travel-time deviations from a 1-D Earth model. The adaptive stacking first applies a move-out correction based on distance through PREM [Dziewonski and Anderson, 1981] and iterates to minimise residual travel-times by maximising the amplitude and coherence of a stack of all traces. We correct for crustal structure on both the source and receiver side and topography on the receiver side by applying travel-time corrections as determined by Crust1.0 [Laske et al., 2012], and for upper mantle structure from the underside of the crust down to 1600 km depth (the shallowest turning depth in our collection) by ray-tracing through the P-wave component of GyPSuM [Simmons et al., 2010] (Supplementary Figures 1 and 2). All travel-time deviations are calculated relative to PREM. The source side correction applied is static and is only used for events shallower than 24 km as this is the thickness of the crustal layer in PREM. Using the crustal thickness and velocities from PREM would, particularly in oceanic regions, be inappropriate for waves travelling through the lithosphere. The crustal and mantle corrections allow us to attribute the remaining travel-time residual to structure at depths greater than 1600 km. Travel-time residuals are plotted at the location and depth of the turning point of the ray as this represents the region in which the ray spends the most time and so has the potential to accumulate the most residual time (Figure 2).

The boundary of the LLSVP is defined by obvious travel-time residual trends. We distinguish between cases where the transition can be clearly identified, i.e. where both positive and negative residuals are separated by zero residual, and where a trend towards the transition is observed, i.e. where there are decreasing or increasing residuals but no change in sign. As the boundary location changes with height, we consider each event individually and separate turning points into a series of 100 km thick radial bins from the CMB upwards. Events with too few turning-points in a height bin to show either the boundary or a trend towards the boundary are discarded.

For each event, we trace the LLSVP boundary in each height bin, with extent controlled by the ray coverage. For each height bin, we then take the boundaries of all events together and define a single boundary which best fits the individual measurements (Figure 3). As an additional measure of the LLSVP boundary, we use the magnitude of the gradient of travel-time residuals. We bin data (in 0.5x0.5° bins) and calculate the average residual. In regions where data fill adjacent bins, we calculate the gradient of the travel-time residuals and choose a boundary defined by a line of highest gradient (Figure 4). Although this method is more robust as it analyses only the pattern of residual travel-times, rather than the absolute value which can be affected by source depth errors, it is only applicable in regions of dense sampling. In comparison, the absolute travel-time residuals can be used to locate the boundary when sampling is poor, but the location will be less well constrained. In general, in well sampled regions the results of both methods agree well.

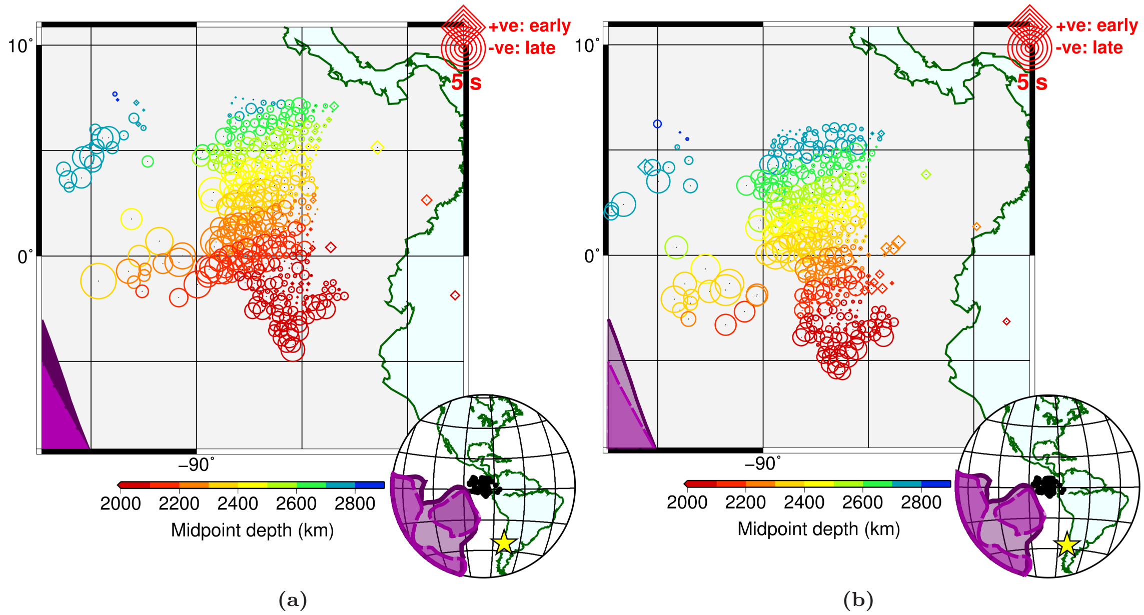

Figure 2: Delay times shown at turning point location and depth for two separate events. Diamonds denote early, and circles show late arrivals (by up to 5 s) indicating fast and slow velocities in the lower mantle, respectively. Events occurring on (a) 28/02/2010 at 34.97° S, 71.69° W at 46.5 ± 4.5 km depth, and (b) on 23/04/2010 at 37.54° S, 72.92° W at 43.1 ± 18.3 km depth. The two events are closely located and sample the same region of the lower mantle. LLSVP contours from GyPSuM are shown as purple lines, as defined in Figure 1. No source-side crustal correction is applied as both events occur below the crust. Inset shows source location as a yellow star, and ray turning points as black circles. [Span 2 columns]

4 Results

We find laterally varying delay times at all depths with some of the largest deviations being seen in the lowermost 300 km of the mantle. We observe patterns of the delay times that are consistent between different source-receiver combinations sampling comparable regions of the lowermost mantle (Figure 2), showing that our method is robust and the delay times are the result of the mantle structure and not artefacts of our processing. The segments of the LLSVP boundary resolved by individual events show very good agreement and excellent continuity between events, allowing the construction of a continuous boundary. The boundary is complex with small scale variations. The resolved P-wave LLSVP boundary is consistent with the shape of the LLSVP boundary as defined in both P- and S-wave tomography models (Figures 3, 5, and Supplementary Figure 3a). The boundary can also be followed in height above the CMB, dependent on ray coverage.

By calculating the gradient of the travel-time residuals and considering both the magnitude (trend of changing travel-time residuals) and its direction, we are better able to observe structure within regions of predominantly fast or slow delay-times. As such, we observe sharp increases in gradient around large negative travel-time residuals within the lower 200 km of the mantle, which are consistently observed in all events sampling the same region. In particular, the northern edge of the LLSVP at $\sim 20°$ N, $\sim 164°$ W (dotted line in Figures 4 and 4c, and the highlighted southern-most points in Figure 6b). These sharply defined regions show travel-time delays of up to 4 s, among the highest detected in this study, relative to the corrected model, and are up to $5°$ wide. Due to the large travel-time anomaly, their small size, and sharp boundaries we interpret these areas as ULVZs.

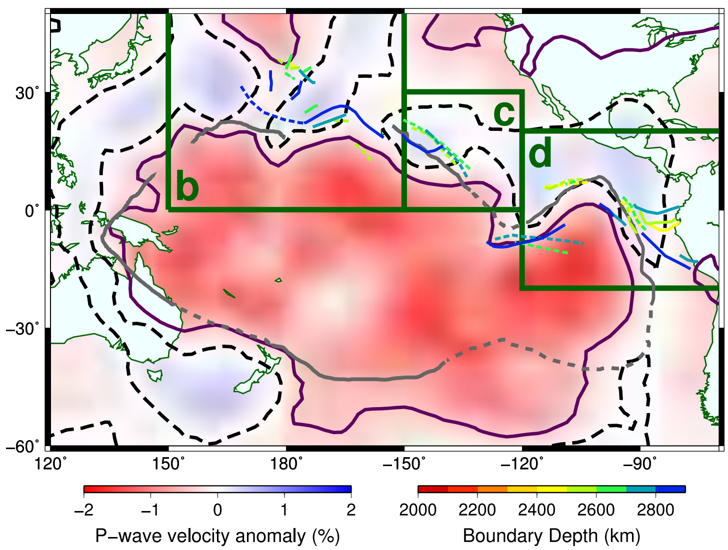

(a)

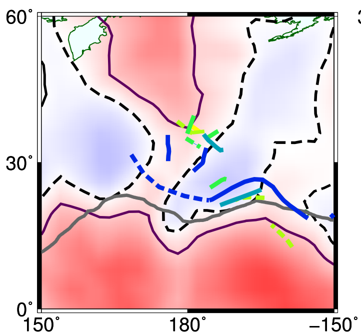

(b)

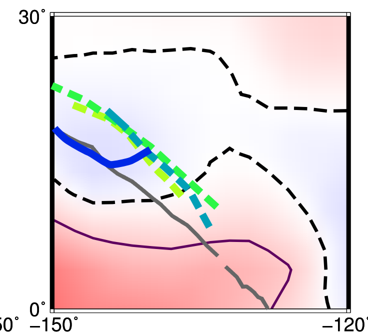

(c)

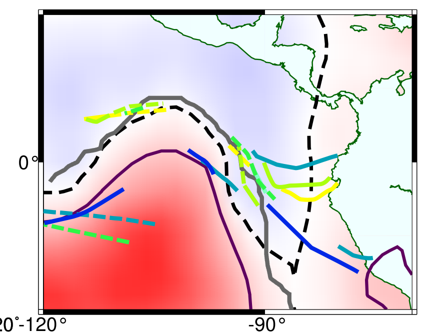

(d)

Figure 3: Location of the P-wave LLSVP boundary determined using the transition from positive to negative travel-time residuals, overlaid on tomography for the lowermost mantle from 2650 km to the CMB (left colour scale) from GyPSuM [Simmons et al., 2010]. (a) LLSVP boundary at various heights (right colour scale). Solid lines show the observed transition and dashed lines indicate where a trend towards the boundary (increasing or decreasing delay times) is observed but the actual transition (as a clear zero delay time) is not seen. The boundary of the Pacific LLSVP determined with S-wave travel-times residuals is shown (grey line) [He and Wen, 2012], along with the -0.4 % and 0.0 % V_P contours in GyPSuM (purple and black dashed lines, respectively) [Simmons et al., 2010]. Three subregions of the travel-time boundary, marked by dark green lines, are shown in greater detail: (b) north-west, (c) north-east, and (d) east. [Span 2 columns]

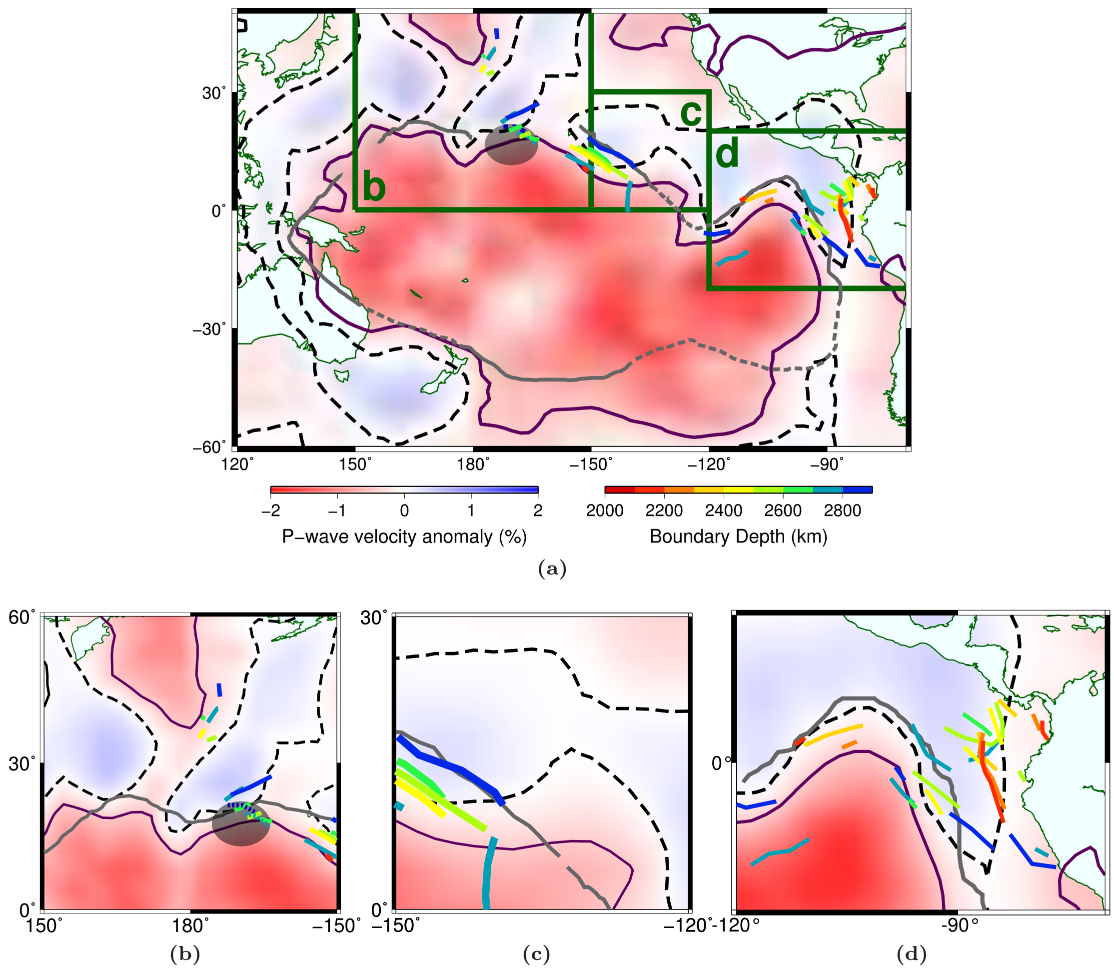

Figure 4: Location of the P-wave LLSVP boundary as in Figure 3 but for delay-time gradients, overlaid on tomography for the lowermost mantle from 2650 km to the CMB (left colour scale) from GyPSuM [Simmons et al., 2010]. (a) LLSVP boundary at various heights (right colour scale). Solid lines show where the boundary is observed, dotted lines and the grey ellipse show the region of a suspected ULVZ characterised by very high velocity gradients. The boundary of the Pacific LLSVP determined with S-waves travel-times residuals is shown (grey line) [He and Wen, 2012], along with the -0.4 % and 0.0 % V_P contours in GyPSuM (purple and black dashed lines, respectively) [Simmons et al., 2010]. Three subregions of the gradient boundary, marked by dark green lines, are shown in greater detail: (b) north-west, (c) north-east, and (d) east. [Span 2 columns]

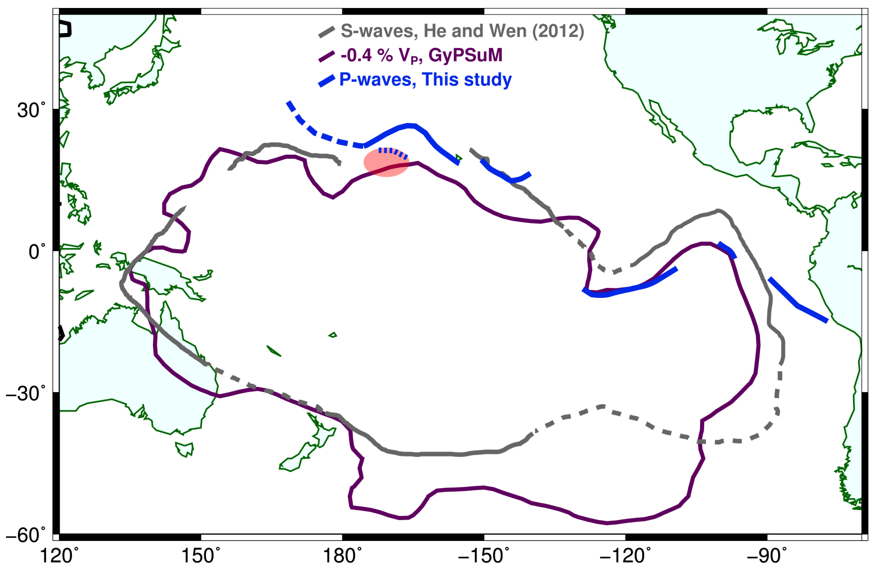

Figure 5: Best fitting P-wave LLSVP boundary determined using travel-time anomalies in the height bin from the CMB to 2800 km depth, as in Figure 3. The LLSVP boundary determined using S-waves [He and Wen, 2012] and the -0.4 % V_P iso-velocity contour from the GyPSuM tomography model [Simmons et al., 2010] are shown as dark grey and purple lines, respectively. The region of a suspected ULVZ, determined from a high travel-time residual gradient in the height bin from the CMB to 2800 km depth, is shown by the dotted blue line and red ellipse.

We use two methods to define the P-wave LLSVP boundary: *(1)* the area of transition between positive and negative travel-time residuals, *(2)* the largest gradient of the travel-time residuals. Often the boundary does appear to be very sharp, with the transition occurring between two turning points, over as little as 40 km (Figures 6a, c, e, and g). This is consistent with the results from S-wave studies for the African LLSVP [Ni et al., 2002]. However, the assumption of a sharp boundary may be inappropriate in some locations; for example, the northern edge of the LLSVP (Figures 6b, d, f, and h) where the boundary appears to be more diffuse. The regions of dominantly positive delays and dominantly negative delays appears to be separated by as much as $\sim 2°$ (120 km) of small, varying positive and negative residual travel-times. Either side of this diffuse boundary region are rapid changes in delay time, to positive and negative delays, respectively, which appear to be straight and near-parallel to each other (drawn as dashed lines in Figures 6b, d, f, h). This may represent a region of material with transitional properties from the LLSVP to ambient mantle or could be generated by multipathing around the edge of the anomaly. Although we do not assess the waveforms further in this paper, we note that there is evidence for wavelet broadening along the northern edge of the LLSVP which is not observed for events sampling the eastern edge. However, this could be due to a smaller range of azimuths available for the eastern side, suggesting that the boundary may not actually be sampled. This is unlikely since the boundary is clearly evident in the travel-time residuals. Alternatively, this region of varying residual sign could be the result of the ray geometry relative to the edge of the LLSVP causing rays to travel through both slower and faster material away from the turning point of the ray. On the eastern side of the LLSVP rays are more likely to travel either outside or inside the LLSVP, but due to the small Fresnel zone of the data are unlikely to travel through both, and so do not show a broad variable region.

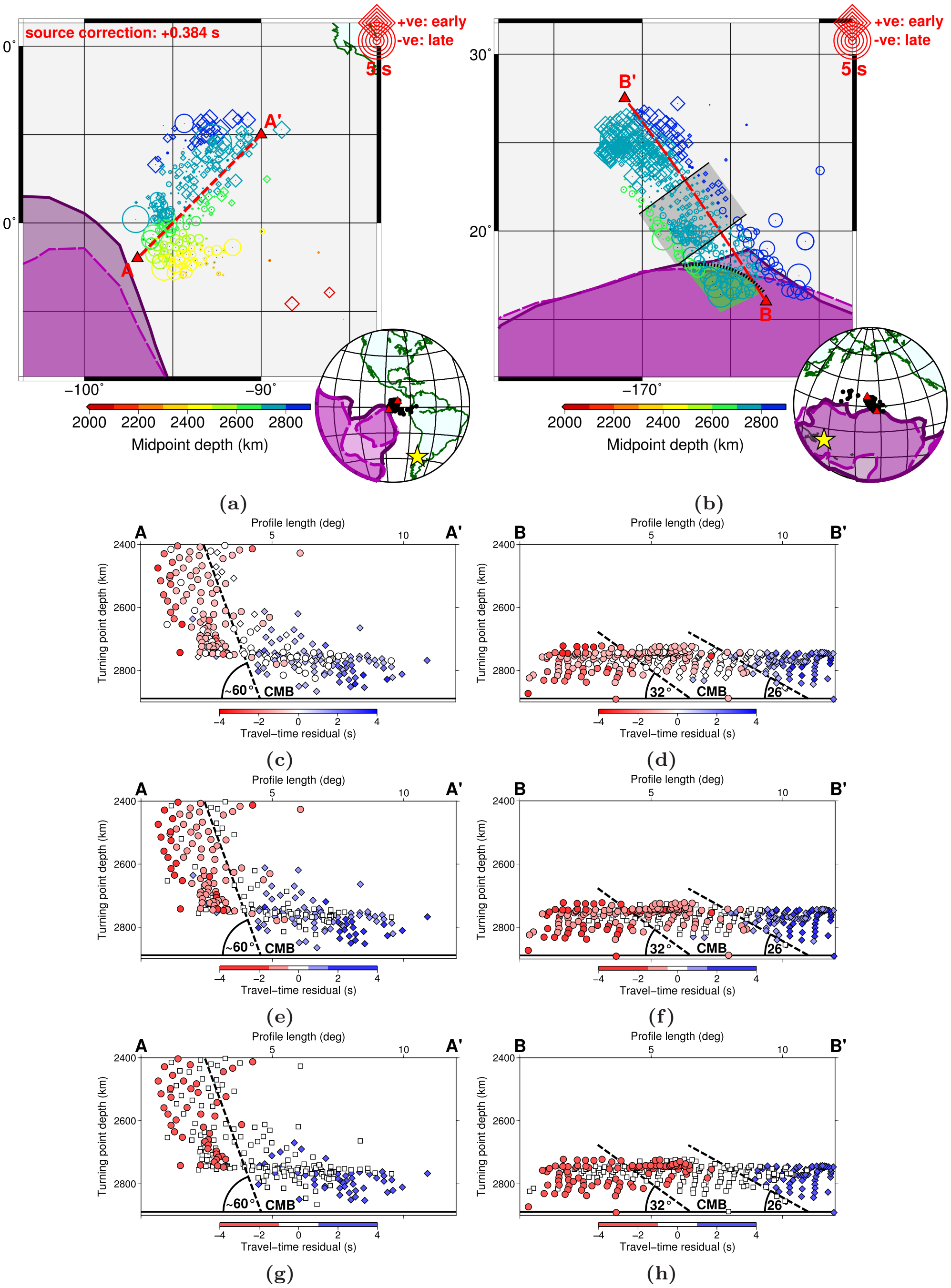

Figure 6: Delay times shown at turning point location and depth. Diamonds denote early, and circles show late arrivals (by up to 5 s) indicating fast and slow velocities in the lower mantle, respectively. Events occurring on (a) 31/12/2006 at 37.97° S, 71.24° W at 47 ±17.1 km depth , and on (b) 01/04/2007 at 8.40° S, 156.94° E at 10 km depth. A region of travel-time residuals with varying sign is indicated by grey shading. A region of strong, negative travel-time residuals, interpreted as the location of a ULVZ, separated from the rest of the delays by a sharp travel-time gradient, is shown by a dotted line with green shading. The -0.4 % V_P iso-velocity contours from GyPSuM at 2500-2650 km and 2650-2900 km (representing the LLSVP boundary) are shown as purple contours and shaded areas, as defined in Figure 1. Inset shows source (star), ray turning points (circles), and cross-section end points (triangles). Cross-sections through turning points along the red section line shown in the maps for events on (c, e, g) 31/12/2006 and (d, f, h) on 01/04/2007. The vertical scale is exaggerated by a factor of 2.7. Figures (c) and (d) show travel-time residuals as symbol colour while figures (e), (f), (g), and (h) use more saturated colour scales to highlight the strongest travel-time variations. Dotted lines separating the fast and slow regions are picked by following pronounced changes in magnitude and sign of the travel-time residuals. Travel-time residuals on the eastern edge of the LLSVP show a sharp transition from positive to negative residuals (c, e, g), whereas the transition is broader on the northern edge with sharp boundaries either side of the transition (d, f, h). Low travel-time residuals (-0.5 to +0.5 s, and -1 to +1 s, for figures (e) and (f), and (g) and (h), respectively) are shown as white squares. However, the transition on the northern edge of the LLSVP close to the CMB is sharp and becomes more diffuse higher above the CMB. [Span 2 columns]

Using residual travel-times determined at different heights, we trace the boundary of the LLSVP from the CMB up to ~500 km above the CMB and ~700 km in some regions (Figures 3 and 4). We observe variations in the steepness of the detected boundary between the east, and the north and north-east sides of the LLSVP, which are the regions best resolved by our data. Using cross sections through the turning points, we are able to visually define the boundary and estimate the slope. We find that the eastern edge is steeper at ~60° (relative to the horizontal) dipping roughly to the north-east, while the northern edge is shallower with slopes between 26 and 32°, dipping north-west (Figures 6c and 6d).

5 Sources of errors

The boundaries of the LLSVP inferred by the P-wave data are very consistent and stable between events (Figure 2) and the crustal and mantle corrections for 3-D velocity heterogeneity correct for most structure along the path above our region of interest. Nonetheless, there are several potential sources of error that might affect the location of the detected boundary of the LLSVP. Due to the source-receiver locations, we have dominant back-azimuths for individual events, which does not allow for crossing paths. The lack of crossing paths might lead to smearing of the travel-time anomaly along the ray path and rays may encounter lower mantle velocity heterogeneity outside the LLSVP which is then mapped to the ray turning point (e.g. Supplementary Figure 1a). There may be additional smearing caused by assuming that the turning point represents the main source of the travel-time anomalies, while the travel-time anomaly is accumulated along the path through the lowermost mantle. This could account for the northern edge of the LLSVP being traced ~10° further north than the -0.4 % contour in the tomography model (Figure 3). The rays in this region will travel through material both slower and faster than PREM, inside and outside of the LLSVP, likely masking the precise point of transition by reducing its apparent magnitude. This problem also affected S-wave studies of the boundary [He and Wen, 2012], and is a possible cause of the good agreement between both studies in this region. Further studies using waveform modelling might help to alleviate the issue. However, the frequencies used here are currently inappropriate for full 3-D wavefield modelling. We note that the boundaries defined using the gradient of the residuals agree well with those determined by the zero crossing of the travel-time residuals in regions where rays travel parallel to the boundary, but plot further towards the centre of the LLSVP than the zero crossing where the ray travels perpendicular to the boundary (Figures 3 and 4).

We use the REB catalogue due to the high quality source locations reported (Supplementary Table 1). Lateral location is, on average, defined to within ±10 km of the published hypocentre. Depth, however, is often less well constrained with half of the events used not having a published depth and those with depths have average errors of ±7 km. Prior to processing, we choose a depth of 10 km for all events where the depth has not been reported in the catalogue. We test the extent to which these depth variations affect the resulting delay-time patterns. For hypocentres within the upper crust, depth uncertainties affect the pattern considerably; for example, between a source at the surface and at 10 km depth, for a ray reaching the CMB, there is ∼1 s travel-time difference relative to the 1-dimensional model taking 3-dimensional corrections into account. However, between sources at 10 km and 20 km depth there is only ∼0.03 s travel-time difference. There is an imperceptible variation in turning point locations in both circumstances. Additionally, the effect on both turning point location and delay time is negligible for events deeper than 10 km. Therefore, source depth uncertainty is only significant for events shallower than 10 km depth. The travel-time shifts that a source depth error would introduce would affect all stations equally and so change the location of the boundary laterally, but the resolved shape of the boundary would be unaltered. The amount by which the boundary would move laterally depends on the gradient of the velocity anomalies around the boundary.

The applied crustal corrections for the source are static. We believe that this is suitable, given that the difference in the section of the crust sampled by two rays, even with vastly different take-off angles and back-azimuths, is negligible when compared to the 1° resolution of the crustal model used [Laske et al., 2012]. Therefore, inaccuracies in the source depth will affect the delay-time for all stations in the same way, increasing or decreasing all delay-times as a DC shift. The transition from positive to negative delay times will be affected, and so will the point at which the boundary is defined. However, the pattern of delays relative to each other will not change. In these situations, therefore, the magnitude of the gradient is a better measure of the location of the LLSVP boundary. Gradients can only be calculated where there are rays sampling adjacent locations. If sampling of the lower mantle is sparse then gradients cannot be determined. Also, care must be taken not to pick sharp changes in gradient resulting from lack of sampling as a boundary, a problem which can be easily avoided when using travel-time residuals.

Body-waves have been shown to be sensitive to off-ray-path structure [Marquering et al., 1998, 1999]. However, this is only significant for intermediate and long period waves. Using high-frequency

P-waves (~1 Hz) with the related small Fresnel zone means that this is irrelevant and ray theory approximation is still valid. The first Fresnel zone for P-waves sampling the lower mantle with a dominant frequency of 1 Hz is ~100-140 km [Sato and Fehler, 2008], equivalent to the distance between 3 stations. This indicates that multi-pathing may affect the exact location at which the LLSVP boundary is defined, but the location will still be accurate to within 2° at the turning point of the ray.

The remaining delay-times, therefore, represent the deviation of the wave arrival time from that predicted by a 3-D tomography model. Any further errors are due to tomography models not sufficiently explaining Earth structure on the scales imaged here and are unavoidable in high frequency studies [Thorne et al., 2013b].

6 Discussion

We map out spatially limited but detailed sections of the P-wave boundary between the Pacific LLSVP and the surrounding mantle. We resolve locally complex structure and boundaries of varying steepness. The location of the boundary generally agrees well with that determined using S-waves [He and Wen, 2012] (Figure 5), not showing any decorrelation of the structure for the different wave types, except for easternmost extent of the boundary. Local variations of the P-wave and S-wave boundaries do not allow the different resolution of these two probes to be compared.

In the north-west (Figures 3b and 4b) the LLSVP boundary slopes fairly shallowly to the north-west. However, ray coverage in this location does not allow the boundary to be traced to depths less than ~2600 km, 300 km above the CMB. At the CMB, the boundary is mapped further north than either the high resolution S-wave study [He and Wen, 2012] or indicated by the 0.0 % or -0.4 % V_P contours in the tomography model. On the other hand, the boundary matches the -0.4 % V_S iso-velocity contour in the S-wave model S40RTS well (Supplementary Figure 3). The difficulty of delineating a well defined boundary from the travel-times in this region that is in agreement with tomographic models might stem from the multiple boundaries determined by the travel-times, possibly due to multipathing effects (Figure 6d). North of the LLSVP (~40° N), a transition is observed from fast material in the south to slower material in the north, consistently observed at a range of depths. This area likely is not sampling the boundary of the main LLSVP but might sample a boundary between subducted material and a smaller low velocity region to the north (Figures 3 and 4), in good agreement with the tomography model. Our study is not conclusive about whether the LLSVP and this northern outlier are completely separate as the boundary of the Pacific LLSVP in this region is defined only as a trend towards the zero crossing, the transition to positive anomalies is not observed. The P-wave tomography model shows a narrow channel of low velocities between the LLSVP and the outlier suggesting that it is not entirely separate. However, this is not supported by the S-wave tomography, in which the outlier does not appear as a coherent feature. This local decorrelation between the P- and S-wave structure may be indicative of this material being compositionally different, or might otherwise indicate different resolution between the tomography models. The northern anomaly may be a smaller or “orphaned” thermo-chemical pile in the process of joining with or separating from the main LLSVP [McNamara et al., 2010, Thorne et al., 2013a].

The determined north-eastern boundary determined here (Figures 3c and 4c) appears to show a steeper vertical dip than in the north-west, and the position agrees well with those determined in the S-wave travel-time study [He and Wen, 2012], and the -0.4 % V_S contour in the S-wave model (Supplementary Figure 3). At this location, the boundary determined by the gradient method is mapped $\sim 10°$ further towards the centre of the LLSVP than the boundary from the travel-time residual method.

At the eastern edge of the LLSVP the boundary becomes steeper and shows a sharp transition from fast to slow material. There is also good agreement between the boundaries determined with both the travel-time residual and gradient methods. At this boundary our study matches well with the S-wave study and also the 0.0 % V_P contour in the tomography model, but our boundary deviates significantly from the -0.4 % V_S contour (Supplementary Figure 3). The boundary in this region is likely the best determined as the ray paths travel parallel to it, hence there will be less contamination from other lower mantle structure, and residual times for rays just grazing the LLSVP will be strongly affected. In this region we are also able to observe the boundary to the greatest height above the CMB ($\sim$700 km) at the northern tip of the eastern extension of the LLSVP. Further east of the LLSVP, close to South and Central America, the boundary begins to deviate more significantly from either the LLSVP as defined by the -0.4 % iso-velocity contour, or the boundary determined by S-waves [He and Wen, 2012]. Our boundary in this region trends east-west along the equator, contrary to other models. Given the consistency of the results using both the travel-time residual and gradient methods in this location (Figures 3 and 4), it seems that the boundary is well defined. However, as the boundary close to South America can be traced to ∼900 km above the CMB (Figure 4), we conclude that this edge is likely not the eastern edge of the Pacific LLSVP but the transition to some other velocity structure and might be related to subduction structures in this region [Garnero and Lay, 2003, Thomas et al., 2004, Hutko et al., 2006, Thorne et al., 2007, Hutko et al., 2009].

Knowledge of the sharpness of the transition will help to resolve arguments about the degree to which lower mantle anomalies are chemical, thermal, or thermo-chemical in nature [Trampert et al., 2004, Davies et al., 2012]. The shape of the LLSVP and the steepness of the walls give can contraints on the viscosity and convective support of these features [Tan and Gurnis, 2005, McNamara and Zhong, 2005, Tan and Gurnis, 2007]. Previous S-wave studies have used waveform modelling to comment on the dip of the boundary [He and Wen, 2009, 2012]. They show the Pacific LLSVP to have both steep and shallow sides on the east and north, respectively, but do not quantify the dip. Their study shows that the western and eastern boundaries are steeper than those reported for the African LLSVP, and the northern boundary of the Pacific LLSVP is reported as shallowly dipping close to the CMB and steeper at greater heights above the CMB. The African LLSVP is shown to also have laterally varying boundary steepness [Ni and Helmberger, 2003a]. The northern edge of the African LLSVP is reported to be steeply overturned [Ni et al., 2002], although other studies show that, despite the boundaries being steep, dipping at between 28 and 70°, they are not overturned [Wen, 2001, Wen et al., 2001, Wang and Wen, 2004, 2007, Helmberger et al., 2009]. In our study we too find boundaries dipping as steeply as that of the African LLSVP and also with lateral variation in the steepness (Figure 6). The eastern edge of the Pacific LLSVP shows an apparent dip of ∼60°, roughly to the north-east, whereas the northern edge is shallower, dipping at between 26 and 32° towards the north-west. However, the boundaries are dependent on the angle at which the cross section is determined across the data points, hence the values stated are apparent dips. Dynamic models of meta-stable, buoyant plumes attempting to take-off from the CMB [Tan and Gurnis, 2005] or a dense, passive body constrained by subduction [McNamara and Zhong, 2005] can both replicate the narrow, curving, and steep-sided nature of the African LLSVP. The Pacific LLSVP's rounder, more dome-like shape, as seen in tomography models, can be generated either by different material properties, relative to the African LLSVP [Tan and Gurnis, 2007], or greater subduction control [McNamara and Zhong, 2005]. Using our technique we have the ability to track the LLSVP and the associated boundary up to ∼700 km above the CMB, matching the heights observed with S-waves [He and Wen, 2012]. However, our data coverage does not allow us to mark out the top of the anomaly and so the complete shape cannot be defined.

Dynamic models imply that active subduction zones could interact with LLSVP, forcing the less viscous thermo-chemical pile laterally, defining location and shape [McNamara and Zhong, 2005]. Therefore, actively subducting slabs may steepen the LLSVP boundary compared to regions where there is no active or recent subduction. We observe that the transition from positive to negative delay times is sharper on the eastern side of the LLSVP than on the northern side (Figure 6), possibly owing to the closer proximity to an active subduction zone on the eastern side. The observation of a steeper eastern edge than northern edge agrees with previous S-wave studies [He and Wen, 2012], indicating that this is a robust observation.

Previously, some studies have reported the LLSVPs to show little to no P-wave velocity change in the lower mantle [Masters et al., 2000, Helmberger and Ni, 2005, Helmberger et al., 2005] where S-wave velocities change more significantly. However, we find substantial P-wave velocity variations: waves with travel-times up to 4 s different than PREM (both slower and faster), with the travel-time perturbation being attributable to the lowermost 1300 km of the mantle. In a simple 1-D calculation of P-wave velocity anomaly, we assume that the Pacific LLSVP is constrained to the lower 500 or 700 km of the mantle (based both on observations by previous studies [He and Wen, 2012] and the overall maximum and local maximum boundary heights in our study, respectively) and that only part of the ray-path (as the turning points are often on the edge of the LLSVP) is contained in the LLSVP and has a constant velocity reduction with depth, in order to fit the observed -4 s travel-time delay. This can be matched with a 700 km thick layer with ΔV_P of -1.5 to -2.5 %, relative to PREM, and a ray travelling through this reduced velocity model for 70 to 50 % of its total length. Alternatively, a 500 km thick layer would have to have ΔV_P of -2.2 to -2.9 %, relative to PREM. However, we accept that this is a grossly simplified calculation and constraining the wavespeed deviation with waveform modelling would be preferable. This consideration notwithstanding, these values are similar to that observed in past studies using P_{diff} passing through the African LLSVP [Wen, 2001, Wen et al., 2001].

The relationship between the P- and S-wave boundaries can help determine the material properties. The ratio of S- to P-wave velocity variations ($R_{S,P}$) is often used as a measure of the degree to which temperature controls the seismic velocites [Robertson and Woodhouse, 1996a,b]. A ratio of $<$2.5 implies that mantle velocity anomalies are dominated by thermal contributions [Karato, 2003], while ratios larger than this imply that chemical variations are also important. Results of comparing tomography models indicate that the seismic velocity of the mantle is dominantly controlled by chemical variations [Robertson and Woodhouse, 1996a,b, Trampert et al., 2004, Della Mora et al., 2011]. However, the validity of this method has been disputed [Schuberth et al., 2009, Davies et al., 2012]. Nonetheless, comparing our 1-D velocity calculation, with $\Delta V_S \sim$-5 % calculated for the Pacific LLSVP [He and Wen, 2012], translates to a V_S/V_P ratio of 1.7 to 3.3. The median value of $\sim$2.4 is higher than other high-frequency lower mantle studies [Wysession et al., 1999, Sun et al., 2007], but agrees with large-scale studies [Robertson and Woodhouse, 1996b, Mosca et al., 2012]. Using this estimate indicates that the Pacific LLSVP, at least in this region, can be explained by a combination of chemical and thermal anomalies [Karato, 2003]. It should be said that this is a maximum estimate for the magnitude of ΔV_P, hence a minimum value of R, and by using either a higher LLSVP height (>700 km) or a longer ray path through the anomaly (perhaps all of the lower mantle) would lead to a smaller ΔV_P. Additionally, this estimate relies on comparing two different studies and using the maximum ΔV_S reported. Using the S-wave information from our dataset processed in a similar way would allow more accurate constraints on the V_S/V_P ratio of the LLSVP.

Superimposed on the large-scale patterns in delay-times, we observe more rapid aberrations in seismic velocities on smaller scales. We see significantly slower seismic velocities in areas previously identified as containing ULVZs [Luo et al., 2001, Cottaar and Romanowicz, 2012], although the magnitude of delay times seen here are smaller than expected for the ULVZ structure, which may be a result from short path-lengths traversing a thin ULVZ. These regions are prominent due to the large delay-time gradient between them and the surrounding slow velocities (Figures 4b and 6b). The strong gradient is in agreement with other core diffracted wave results [Rost and Garnero, 2006]. The location of this ULVZ at the boundary of the LLSVP supports the hypothesis that ULVZs are predominantly found at the edges of, or just within, the LLSVPs [McNamara et al., 2010].

In addition to low velocities (as indicated by negative residuals) we find consistent areas of faster velocities (positive residuals) restricted to the lowermost mantle along the coast of Mexico and South America. This agrees well with many previous studies [Garnero and Lay, 2003, Thomas et al., 2004, Hutko et al., 2006, Thorne et al., 2007, Hutko et al., 2009] showing faster velocities related to subduction of the Farallon slab. As subduction is a top down process it may explain why we see the transition between slow and fast residuals at greater heights in this region than anywhere else in our study (Figure 4d).

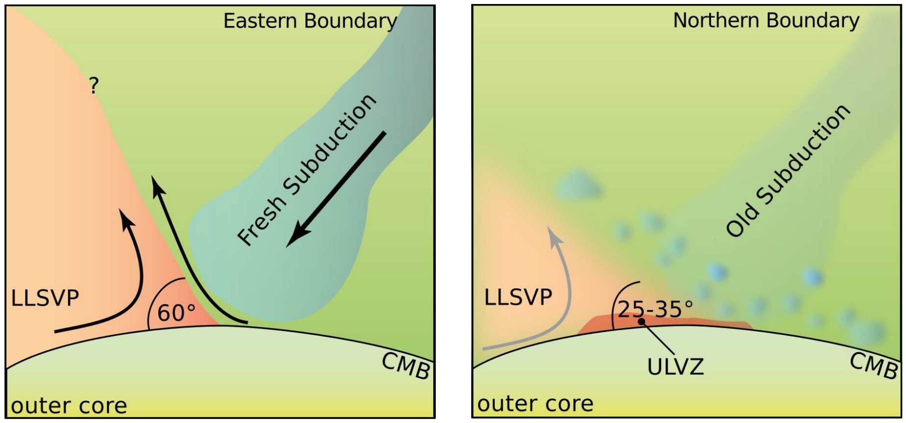

(a) (b)

Figure 7: Conceptual representation of the relationship between LLSVP structure and subduction processes. (a) The observed steep (60° dip), sharp (∼60 km) LLSVP boundary in the east may be caused by recently subducted slab material increasing the thermal gradient and shaping the LLSVP. (b) The shallower (26 to 32°) and more diffuse (∼120 km) northern boundary, by contrast, may be due to the absence of recent subduction.

We propose that the boundary width, or sharpness, and steepness is related to mantle dynamics (Figure 7). In the eastern Pacific, where there are active subduction zones, the boundary is seismically sharp, occurring over 60 km or less, although resolution is limited by the size of the Fresnel zone. In contrast, the northern edge of the Pacific LLSVP has a broader seismic boundary and is further from an active subduction zone. Subducted material that has been present in the lower mantle for longer will have had longer to thermally, and possibly chemically, equilibrate with ambient conditions through conduction and mechanical mixing, respectively. This would lead to a lower gradient (both thermal and compositional) across the boundary which may present as a lower seismic velocity gradient, hence a wider boundary. Conversely, regions of active subduction where crust has recently been subducted, such as the eastern edge of the Pacific LLSVP, would have higher thermal gradients and, therefore, higher seismic delay-time gradients.

7 Conclusion

We use P-wave travel-time delays relative to a tomography model to map out the northern and eastern edges of the Pacific LLSVP from the CMB to 700 km above, and other lower mantle structures up to 900 km above the CMB. The northern and eastern regions show contrasting structures: the northern boundary has a seismically broad transition with a shallow slope (∼120 km wide and a dip of 26 to 32° relative to the horizontal), while the eastern boundary is sharper with a steep slope (∼60 km wide and dipping at 60°). We attribute this to the proximity of the eastern edge to active subduction, steepening and sharpening the boundary through viscous forcing and an increased thermal and/or compositional gradient. Calculation of the V_S to V_P ratio to explore the thermal or compositional origin of the LLSVP is complicated by limited data and the result is inconclusive. Contrary to patterns observed in P-wave and bulk-sound tomography models, the P-wave boundary closely matches that determined with S-wave travel times and the 0.0 % V_P and -0.4 % V_S iso-velocity contours in the GyPSuM and S40RTS models, respectively.

8 Supplementary material

Corrections are applied to travel-times calculated for rays using PREM to account for 3-D mantle structure and crustal heterogeneity on the source and receiver sides. We use the GyPSuM P-wave tomography model [Simmons et al., 2010] and CRUST1.0 model [Laske et al., 2012] (Figures 1 and 2). Mantle corrections are applied for each source-receiver combination, receiver-side crustal corrections are applied for each station, and source-side crustal corrections are applied as a DC shift to events that are shallower than 24 km depth, the average thickness of the crust in oceanic regions in CRUST1.0. Smearing of mantle heterogeneity along the ray-path is apparent as significant negative corrections are applied at ray turning points outside the tomographic extent of the Pacific LLSVP.

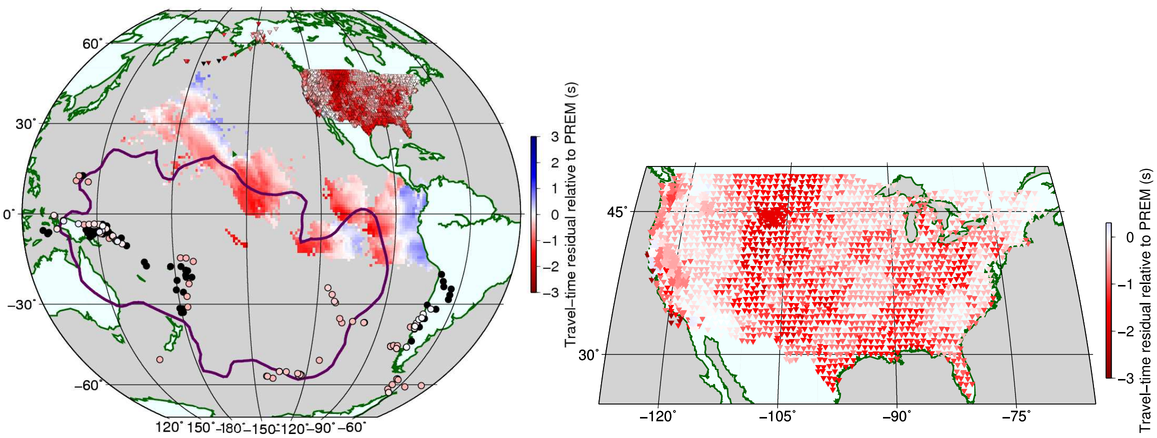

(a) (b)

Supplementary Figure 1: Crustal and mantle corrections relative to PREM for (a) the whole path and (b) and at each station. Circles show corrections for crustal structure at the source. Black circles indicate sources deeper than 24 km to which no source-side crustal correction is applied. Triangles show corrections for crustal structure at each station in USArray, averaged over all events which use the station. Background shows corrections for mantle structure along the whole ray-path at the turning point of each ray, averaged over all rays. Crustal structure is determined from CRUST1.0 [Laske et al., 2012] and mantle structure is determined from the P-wave component of the GyPSuM model [Simmons et al., 2010]. The -0.4 % V_P contour from GyPSuM is shown by the purple line.

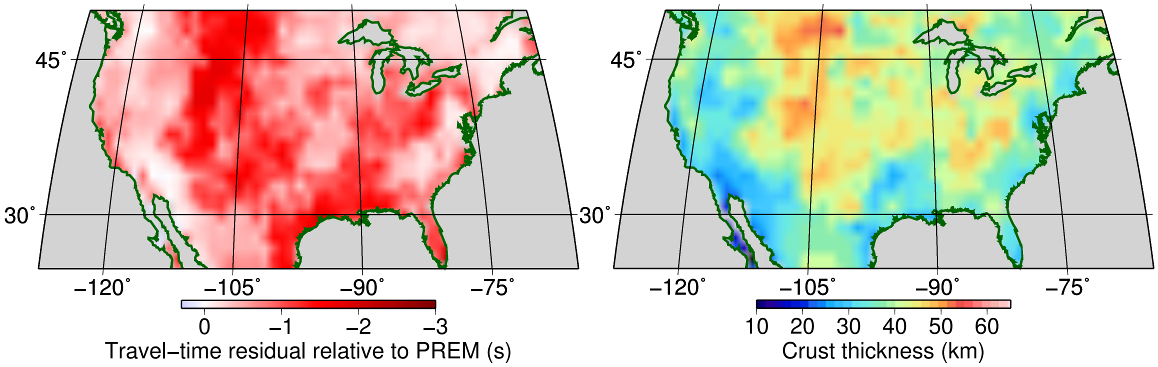

(a) **(b)**

Supplementary Figure 2: Crustal structure taken from CRUST1.0 [Laske et al., 2012]. (a) Travel times and (b) crustal thickness in each 1x1° cell.

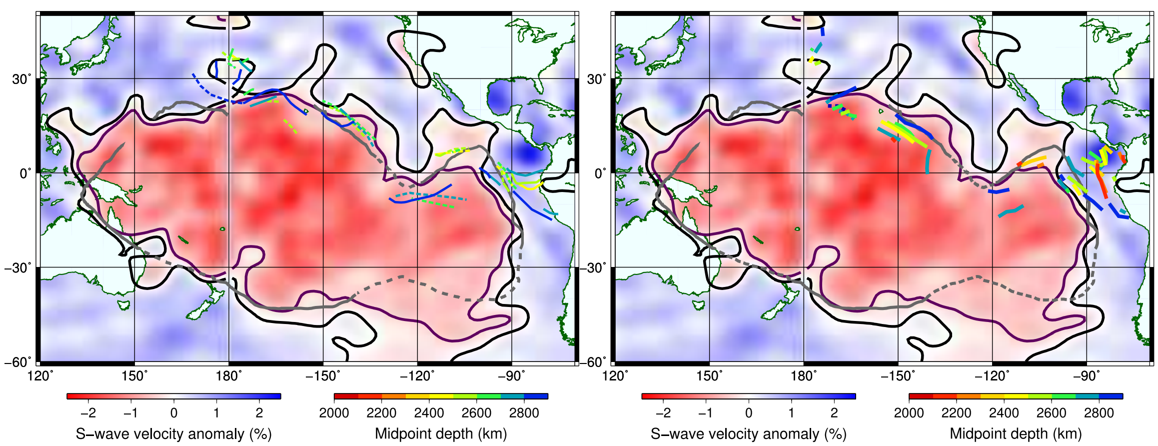

(a) **(b)**

Supplementary Figure 3: Location of the P-wave LLSVP boundary determined in our study, overlaid on S-wave tomography for the lowermost mantle from 2800 km to the CMB from S40-RTS [Ritsema et al., 2011]. (a) LLSVP boundary at various heights drawn from the transition from positive to negative delay times. Solid lines show where the transition is observed and dashed lines indicate where a trend towards the boundary (increasing or decreasing delay times) is observed but the actual transition is not seen. (b) LLSVP boundary determined by regions of high delay-time gradient. Solid lines show where the boundary is observed, dotted lines show regions of suspected ULVZs characterised by very high velocity gradients. The boundary of the Pacific LLSVP determined with S-waves travel-times residuals is shown (grey line) [He and Wen, 2012], along with the -0.4 % and 0 % V_P contours in S40-RTS (purple and black line, respectively) [Ritsema et al., 2011].

Table 1: Events in dataset reported in the REB catalogue. Events at 0 km depth are assigned a depth of 10 km before being processed.

Date	Origin Time	Latitude	Longitude	Depth (km)	Error (km)	Mag.	Mag. Type
2004/01/29	03:52:50.60	-50.2311	-114.5760	0.0	0.0	5.9	Ms1
2004/05/03	04:36:46.17	-37.6975	-73.4590	0.0	0.0	6.7	Ms1
2004/06/02	08:50:38.58	-32.8080	-179.2670	50.7	17.3	5.7	Ms1
2004/06/15	11:16:32.16	-38.7379	-73.0550	40.8	4.0	5.6	Ms1
2004/08/28	13:41:33.01	-35.0085	-70.5490	32.1	16.4	6.5	Ms
2004/11/28	02:35:11.03	-26.6375	-113.8760	0.0	0.0	6.2	Ms1
2004/12/23	14:59:03.00	-49.9522	161.1740	0.0	0.0	7.7	Ms1
2005/01/16	20:17:48.72	10.8665	140.8750	0.0	0.0	6.5	Ms1
2005/01/22	20:30:17.20	-7.8927	159.4700	24.9	9.1	6.4	Ms1
2005/03/02	10:42:11.08	-6.5018	129.8800	196.9	4.0	6.9	mbtmp
2005/03/21	12:23:54.22	-24.8201	-63.4030	580.4	3.9	6.4	mbtmp
2005/05/12	11:15:33.11	-57.3256	-139.1500	0.0	0.0	6.3	Ms1
2005/06/02	10:56:00.50	-24.0577	-66.8760	185.6	3.3	5.8	mbtmp
2005/06/04	14:50:48.66	-6.3735	146.8450	39.4	9.2	5.8	Ms1
2005/06/13	22:44:32.79	-19.9043	-69.1240	109.6	2.3	7.2	Ms1
2005/06/15	10:13:55.10	-4.5417	153.2100	37.2	7.1	5.7	mbtmp
2005/06/15	19:52:22.86	-44.9612	-80.6860	0.0	0.0	5.9	Ms1
2005/07/10	04:46:29.50	-36.3517	-97.3350	0.0	0.0	5.7	Ms
2005/08/07	11:35:24.31	-14.4012	-177.1970	0.0	0.0	5.7	Ms1
2005/09/05	07:37:28.13	-56.5051	-142.2550	0.0	0.0	5.8	Ms1
2005/09/09	07:26:43.76	-4.5031	153.3150	95.6	20.1	7.0	Ms1
2005/09/29	15:50:20.47	-5.3781	151.8760	0.0	0.0	6.5	Ms1
2005/11/17	19:26:55.32	-22.2588	-67.6840	151.4	2.6	6.2	mbtmp
2005/11/22	15:11:33.18	-5.1855	145.3930	82.6	19.4	5.7	mbtmp
2005/12/11	14:20:46.41	-6.5837	152.1870	24.6	10.0	6.2	Ms1
2005/12/11	14:20:46.41	-6.5837	152.1870	24.6	10.0	6.2	Ms1
2006/01/27	16:58:51.75	-5.4244	128.1500	378.0	3.3	7.0	mbtmp
2006/03/05	08:07:55.27	-20.1441	-175.7220	195.5	8.1	6.1	mbtmp
2006/03/10	10:12:17.18	-60.4068	-46.5340	0.0	0.0	5.4	Ms1
2006/05/16	10:39:20.74	-31.5728	-179.1710	122.0	6.9	6.8	Ms1
2006/08/07	22:18:56.53	-15.7922	167.7890	161.8	5.3	6.5	mbtmp
2006/09/01	10:18:55.21	-6.7815	155.4540	70.1	10.0	6.5	Ms1
2006/09/01	10:18:55.21	-6.7815	155.4540	70.1	10.0	6.5	Ms1
2006/09/17	09:34:13.04	-31.7291	-67.1010	136.4	1.8	5.7	mbtmp
2006/10/10	08:02:49.82	-56.1238	-122.5430	0.0	0.0	5.8	Ms1
2006/10/17	01:25:17.62	-5.9881	151.0560	77.4	9.0	6.7	Ms1
2006/10/17	01:25:17.62	-5.9881	151.0560	77.4	9.0	6.7	Ms1
2006/11/07	17:38:31.75	-6.4324	151.2520	0.0	0.0	6.2	Ms1
2006/12/27	20:15:39.64	-5.8304	154.3310	361.8	6.3	5.4	mb1
2006/12/31	14:55:05.96	-37.9745	-71.2400	47.0	17.1	5.0	mb1mx
2007/01/17	18:34:13.73	-57.9826	-64.4700	0.0	0.0	5.7	ML
2007/02/04	21:17:42.58	-55.6693	-123.5230	0.0	0.0	5.9	Ms1
2007/02/10	06:03:02.85	-43.0439	-71.7370	160.2	3.8	4.8	mb1
2007/03/31	12:49:01.60	-55.8618	-123.4770	0.0	0.0	6.1	Ms1
2007/04/01	20:39:55.04	-8.4009	156.9350	0.0	0.0	7.5	Ms1

Table 1: Events in dataset reported in the REB catalogue. Events at 0 km depth are assigned a depth of 10 km before being processed.

Date	Origin Time	Latitude	Longitude	Depth (km)	Error (km)	Mag.	Mag. Type
2007/04/01	20:39:55.04	-8.4009	156.9350	0.0	0.0	7.5	Ms1
2007/04/01	20:47:29.24	-7.1990	156.0660	0.0	0.0	7.4	Ms1
2007/04/01	21:11:31.75	-7.3166	155.8140	0.0	0.0	7.0	Ms1
2007/04/02	02:49:39.75	-45.3134	-72.6630	25.7	15.5	5.7	Ms1
2007/04/13	18:24:17.83	-34.9579	-108.9980	0.0	0.0	5.7	Ms1
2007/04/21	17:53:42.31	-45.2236	-72.6390	10.8	7.0	6.2	Ms1
2007/05/07	11:15:14.23	-44.9415	-80.7710	0.0	0.0	5.7	ML
2007/05/29	01:03:27.43	-4.6293	151.7550	128.9	2.5	5.3	mb1mx
2007/06/07	00:40:39.05	-3.3887	146.7150	8.2	10.5	6.0	Ms1
2007/06/28	02:52:07.64	-8.0099	154.5230	0.0	0.0	6.4	Ms1
2007/08/16	08:39:25.68	-9.8066	159.5920	0.0	0.0	6.4	Ms1
2007/09/07	04:46:44.38	-56.0433	-124.0470	0.0	0.0	5.0	Ms
2007/09/26	12:36:20.67	-4.8338	153.6490	0.0	0.0	6.1	Ms1
2007/09/30	02:08:28.01	10.4573	145.7800	0.0	0.0	6.9	Ms1
2007/10/05	07:17:51.80	-25.1189	179.4870	497.7	5.0	5.3	mb1mx
2007/11/22	08:48:30.51	-5.7972	147.0560	74.8	18.2	6.4	Ms1
2007/11/29	03:26:21.83	-36.3826	-97.5820	0.0	0.0	5.5	Ms
2007/12/09	07:28:14.43	-25.8822	-177.6450	89.9	11.0	6.9	Ms1
2007/12/11	17:20:54.17	-61.8796	-65.2910	0.0	0.0	5.6	ML
2008/01/15	17:52:16.89	-21.8985	-179.5820	601.9	2.6	5.4	mb1
2008/05/09	21:51:31.73	12.5419	143.2430	92.9	3.3	6.2	Ms1
2008/05/20	15:16:04.88	-44.7011	-77.5730	0.0	0.0	5.0	Ms
2008/06/03	16:20:51.58	-10.4437	161.3370	91.6	3.6	5.7	mb1
2008/06/15	08:37:15.97	-36.4449	-107.6950	0.0	0.0	5.3	Ms
2008/06/26	21:19:15.71	-20.8343	-173.2930	38.3	3.7	6.2	ML
2008/07/19	22:39:52.68	-17.2961	-177.3120	387.0	2.9	5.6	mb1
2008/10/22	12:55:57.80	-18.5290	-175.5300	233.1	4.5	5.7	mb1
2008/11/04	18:35:45.24	-17.1211	168.4500	202.9	4.7	5.3	mb
2008/12/09	06:24:01.42	-30.9751	-176.8570	0.0	0.0	6.6	Ms1
2009/01/03	19:43:48.91	-0.4922	132.7570	0.0	0.0	7.3	Ms1
2009/01/03	22:33:36.40	-0.7239	133.1330	0.0	0.0	7.2	Ms1
2009/02/18	21:53:41.29	-27.3387	-176.3580	0.0	0.0	7.1	Ms1
2009/03/19	18:17:35.76	-23.0141	-174.7350	0.0	0.0	7.4	Ms1
2009/05/12	01:26:27.11	-5.6724	149.4650	96.3	2.5	5.5	mb1
2009/06/23	14:19:22.02	-5.2054	153.7170	96.2	3.4	6.2	Ms1
2009/07/08	19:23:35.97	-35.9498	-102.8730	0.0	0.0	5.3	mb1
2009/07/15	20:10:39.80	-3.3882	150.6430	0.0	0.0	5.9	Ms1
2009/08/01	13:33:27.99	-56.2785	-124.2160	0.0	0.0	5.4	Ms
2009/09/17	23:21:38.15	-28.9814	-112.5610	0.0	0.0	6.0	Ms1
2009/09/29	17:48:08.06	-15.5716	-172.0830	0.0	0.0	8.0	Ms1
2009/10/14	18:00:22.01	-14.5033	-174.9490	0.0	0.0	5.9	Ms1
2009/10/24	14:40:46.23	-6.0643	130.4240	151.0	7.0	6.3	Ms1
2009/10/27	00:04:44.61	-59.9575	-65.1980	0.0	0.0	5.6	ML
2009/11/09	10:44:53.17	-17.2944	178.4080	571.8	6.1	5.8	mb1
2009/11/22	22:47:28.62	-31.4545	179.5500	440.8	3.5	5.9	mbtmp
2009/12/03	06:12:30.93	-56.0247	-122.7040	0.0	0.0	5.7	Ms1

Table 1: Events in dataset reported in the REB catalogue. Events at 0 km depth are assigned a depth of 10 km before being processed.

Date	Origin Time	Latitude	Longitude	Depth (km)	Error (km)	Mag.	Mag. Type
2010/01/03	21:48:01.74	-8.6247	157.3590	0.0	0.0	6.1	Ms1
2010/01/03	22:36:25.04	-8.6752	157.2140	0.0	0.0	6.8	Ms1
2010/01/05	12:15:29.80	-8.9872	157.4440	0.0	0.0	6.4	Ms1
2010/01/05	13:11:37.71	-8.9551	157.8000	0.0	0.0	5.7	Ms1
2010/01/17	12:00:00.45	-57.6703	-65.7130	0.0	0.0	5.8	Ms1
2010/02/27	06:51:11.48	-31.7032	-69.3140	0.0	0.0	6.3	ML
2010/02/27	07:37:17.99	-36.9396	-72.8060	34.5	3.1	5.7	mbtmp
2010/02/27	08:01:17.05	-37.9535	-75.3880	0.0	0.0	7.3	Ms1
2010/02/27	19:00:02.08	-33.3888	-71.8960	0.0	0.0	5.9	Ms1
2010/02/27	23:12:29.89	-34.7288	-71.8660	0.0	0.0	5.5	mb1
2010/02/28	11:25:35.88	-34.9714	-71.6710	46.5	4.6	5.8	mbtmp
2010/03/03	17:44:21.89	-36.6233	-73.3770	0.0	0.0	5.8	Ms1
2010/03/20	14:00:52.76	-3.4000	152.1700	437.8	10.4	6.2	mbtmp
2010/03/20	14:00:52.76	-3.4000	152.1700	437.8	10.4	6.2	mbtmp
2010/04/17	23:15:26.20	-6.6419	147.2790	87.4	7.3	5.9	mbtmp
2010/04/23	10:03:07.76	-37.5376	-72.9210	43.1	18.3	5.6	Ms1
2010/05/19	10:30:08.40	-54.5737	-135.5050	0.0	0.0	5.5	Ms
2010/05/19	10:51:01.58	-54.6125	-135.4730	0.0	0.0	5.7	Ms1
2010/06/16	03:16:25.82	-2.1010	136.4420	0.0	0.0	6.9	Ms1
2010/06/16	03:58:06.35	-2.2787	136.6280	0.0	0.0	6.4	Ms1
2010/06/17	13:06:53.26	-32.9068	179.8190	222.6	7.7	5.9	mbtmp
2010/07/14	08:32:17.61	-38.1215	-73.4290	0.0	0.0	6.5	Ms1
2010/07/18	13:04:11.14	-5.9808	150.5960	35.9	6.2	6.8	Ms1
2010/07/18	13:35:00.00	-5.9208	150.8270	0.0	0.0	7.0	Ms1
2010/08/04	07:15:33.19	-5.5067	146.8260	217.4	4.2	6.1	mbtmp
2010/08/04	07:15:33.19	-5.5067	146.8260	217.4	4.2	6.1	mbtmp
2010/08/04	22:01:36.91	-5.7719	150.7910	0.0	0.0	6.4	Ms1
2010/08/13	21:19:30.54	12.5029	141.7080	0.0	0.0	6.8	Ms1
2010/08/15	15:09:29.23	-5.7334	148.3550	174.2	2.1	6.1	mbtmp
2010/09/29	17:11:20.53	-4.9226	133.7800	0.0	0.0	6.7	Ms1
2010/10/30	15:18:28.87	-56.4651	-142.8330	0.0	0.0	5.5	Ms
2010/11/21	04:36:29.26	-54.7245	-131.6020	0.0	0.0	5.5	Ms1
2010/12/02	03:12:11.68	-5.9849	149.8600	43.8	5.7	6.3	Ms1
2011/01/01	09:56:59.13	-26.8215	-63.2420	587.1	2.3	6.8	mbtmp
2011/01/02	20:20:13.41	-38.4370	-73.2710	0.0	0.0	7.0	Ms1
2011/02/12	17:57:56.56	-20.8429	-175.6110	86.8	9.4	5.8	mbtmp
2011/03/01	00:53:44.52	-29.5026	-111.9880	0.0	0.0	5.8	Ms1
2011/05/15	18:37:11.44	-6.0992	154.4540	49.0	12.7	5.9	mbtmp
2011/06/01	12:55:18.92	-37.6025	-73.6960	0.0	0.0	6.3	Ms1
2011/07/31	23:38:54.94	-3.4978	144.7360	0.0	0.0	6.6	Ms1
2011/08/28	10:10:17.17	-24.3776	-115.9510	0.0	0.0	5.2	Ms1
2011/09/02	13:47:11.06	-28.4251	-63.1350	590.8	2.6	6.5	mbtmp
2011/10/14	03:35:14.46	-6.5551	147.9330	37.1	8.4	6.2	Ms1
2011/11/11	10:41:34.34	-55.4129	-125.0210	0.0	0.0	5.2	Ms1
2011/12/14	05:04:59.64	-7.5434	146.8700	142.1	4.0	6.6	mbtmp
2012/01/15	13:40:19.50	-60.9176	-55.9400	0.0	0.0	5.6	mb1

Table 1: Events in dataset reported in the REB catalogue. Events at 0 km depth are assigned a depth of 10 km before being processed.

Date	Origin Time	Latitude	Longitude	Depth (km)	Error (km)	Mag.	Mag. Type
2012/03/21	22:15:07.78	-6.2051	146.0330	132.8	9.0	6.2	mbtmp
2012/04/14	10:56:16.88	-57.5568	-65.4750	0.0	0.0	6.0	Ms1
2012/04/17	07:13:50.83	-5.5176	147.1360	209.6	3.2	6.5	mbtmp
2012/04/28	10:08:08.02	-18.6560	-174.7240	128.6	3.8	6.2	mbtmp
2012/05/18	02:00:36.02	-44.9077	-80.6110	0.0	0.0	6.0	ML
2012/07/28	20:03:56.36	-4.6632	153.2280	33.6	4.5	6.0	mbtmp
2012/11/13	04:31:24.84	-45.7464	-77.2260	0.0	0.0	5.7	Ms1
2012/12/29	07:59:14.00	-3.2956	148.8270	0.0	0.0	5.4	Ms
2013/01/23	07:42:56.12	-44.6692	-79.5140	0.0	0.0	4.6	ms1mx
2013/03/10	22:51:52.87	-6.7060	148.2180	53.9	8.0	6.3	Ms1
2013/04/14	01:32:22.04	-6.4404	154.6930	26.7	8.1	6.2	Ms1
2013/04/16	22:55:25.38	-3.2048	142.5110	0.0	0.0	6.1	Ms1
2013/04/23	23:14:37.91	-3.8833	152.2390	0.0	0.0	6.0	Ms1
2013/05/20	09:49:01.19	-44.9980	-80.7190	0.0	0.0	5.6	Ms1
2013/07/07	18:35:31.48	-3.9861	153.8650	394.0	2.9	6.0	mbtmp
2013/07/07	18:35:31.48	-3.9861	153.8650	394.0	2.9	6.0	mbtmp
2013/07/07	20:30:07.45	-6.0104	149.8370	62.4	2.3	5.9	Ms1
2013/07/16	19:41:51.99	-63.3242	-62.3530	0.0	0.0	5.3	mb1mx

References

Thorsten W Becker, James B Kellogg, and Richard J O Connell. Thermal constraints on the survival of primitive blobs in the lower mantle. *Earth Planet. Sci. Lett.*, 171:351–365, 1999.

M Boyet and R W Carlson. 142Nd evidence for early (>4.53 Ga) global differentiation of the silicate Earth. *Science*, 309(5734):576–81, July 2005. ISSN 1095-9203. doi: 10.1126/science.1113634. URL `http://www.ncbi.nlm.nih.gov/pubmed/15961629`.

J. P. Brandenburg and P. E. van Keken. Deep storage of oceanic crust in a vigorously convecting mantle. *Journal of Geophysical Research*, 112(B6):B06403, June 2007. ISSN 0148-0227. doi: 10.1029/2006JB004813. URL `http://doi.wiley.com/10.1029/2006JB004813`.

Kevin Burke, Bernhard Steinberger, Trond H. Torsvik, and Mark A. Smethurst. Plume Generation Zones at the margins of Large Low Shear Velocity Provinces on the coremantle boundary. *Earth and Planetary Science Letters*, 265(1-2): 49–60, January 2008. ISSN 0012821X. doi: 10.1016/j.epsl.2007.09.042. URL `http://linkinghub.elsevier.com/retrieve/pii/S0012821X07006036`.

R.W. Carlson and M. Boyet. Long-term consequences of early Earth differentiation. *Geochimica et Cosmochimica Acta*, 70(18):A84, August 2006. ISSN 00167037. doi: 10.1016/j.gca.2006.06.080. URL `http://linkinghub.elsevier.com/retrieve/pii/S0016703706003590`.

P Castillo. The Dupal anomaly as a trace of the upwelling lower mantle. *Nature*, 336:667–670, 1988.

Ulrich R Christensen and Albrecht W Hofmann. Segregation of subducted oceanic crust in the convecting mantle. *J. Geophys. Res.*, 99:19,867–19,844, 1994.

Sanne Cottaar and Barbara Romanowicz. An unusually large ULVZ at the base of the mantle near Hawaii. *Earth and Planetary Science Letters*, 355-356:213–222, November 2012. ISSN 0012821X. doi: 10.1016/j.epsl.2012.09.005. URL `http://linkinghub.elsevier.com/retrieve/pii/S0012821X12005006`.

Christopher J Davies, David Gubbins, Ashley P Willis, and Peter K Jimack. Time-averaged paleomagnetic field and secular variation : Predictions from dynamo solutions based on lower mantle seismic tomography. *Phys. Earth Planet. Int.*, 169:194–203, 2008. doi: 10.1016/j.pepi.2008.07.021.

D Rhodri Davies, S Goes, J H Davies, B S A Schuberth, H Bunge, and J Ritsema. Reconciling dynamic and seismic models of Earth's lower mantle: The dominant role of thermal heterogeneity. *Earth and Planetary Science Letters*, 353-354:253–269, 2012. ISSN 0012-821X. doi: 10.1016/j.epsl.2012.08.016. URL `http://dx.doi.org/10.1016/j.epsl.2012.08.016`.

S. Della Mora, L. Boschi, P. J. Tackley, T. Nakagawa, and D. Giardini. Low seismic resolution cannot explain S/P decorrelation in the lower mantle. *Geophysical Research Letters*, 38:L12303, June 2011. ISSN 00948276. doi: 10.1029/2011GL047559. URL `http://doi.wiley.com/10.1029/2011GL047559`.

C DeMets, R G Gordon, D F Argus, and S Stein. Current plate motions. *Geophys. J. Int.*, (101): 425–478, 1990.

Frédéric Deschamps, Laura Cobden, and Paul J. Tackley. The primitive nature of large low shear-wave velocity provinces. *Earth and Planetary Science Letters*, 349-350:198–208, October 2012. ISSN 0012821X. doi: 10.1016/j.epsl.2012.07.012. URL `http://linkinghub.elsevier.com/retrieve/pii/S0012821X12003718`.

B. Dupre and C. J. Allegre. Pb-Sr isotope variation in Indian Ocean basalts and mixing phenomena. *Nature*, 303:142–146, 1983.

Adam M Dziewonski. Mapping the Lower Mantle : Determination of Lateral Heterogeneity in P Velocity up to Degree and Order 6. *J. Geophys. Res.*, 89:5929–5952, 1984.

Adam M. Dziewonski and Don L. Anderson. Preliminary reference Earth model. *Physics of the Earth and Planetary Interiors*, 25(4):297–356, June 1981. ISSN 00319201. doi: 10.1016/0031-9201(81)90046-7. URL `http://linkinghub.elsevier.com/retrieve/pii/0031920181900467`.

Sean R. Ford, Edward J. Garnero, and Allen K. McNamara. A strong lateral shear velocity gradient and anisotropy heterogeneity in the lowermost mantle beneath the southern Pacific. *Journal of Geophysical Research*, 111(B3):1–14, 2006. ISSN 0148-0227. doi: 10.1029/2004JB003574. URL `http://www.agu.org/pubs/crossref/2006/2004JB003574.shtml`.

D. A. Frost, S. Rost, N. D. Selby, and G. W. Stuart. Detection of a tall ridge at the core-mantle boundary from scattered PKP energy. *Geophysical Journal International*, 195(1):558–574, July 2013. ISSN 0956-540X. doi: 10.1093/gji/ggt242. URL `http://gji.oxfordjournals.org/cgi/doi/10.1093/gji/ggt242`.

Edward J Garnero and Donald V Helmberger. A very slow basal layer underlying large-scale low-velocity anomalies in the lower mantle beneath the Pacific : evidence from core phases. *Phys. Earth Planet. Int.*, 9201:161–176, 1995.

Edward J. Garnero and Thorne Lay. D shear velocity heterogeneity, anisotropy and discontinuity structure beneath the Caribbean and Central America. *Physics of the Earth and Planetary Interiors*, 140(1-3):219–242, November 2003. ISSN 00319201. doi: 10.1016/j.pepi.2003.07.014. URL `http://linkinghub.elsevier.com/retrieve/pii/S0031920103001742`.

Edward J Garnero and Allen K McNamara. Structure and dynamics of Earth's lower mantle. *Science*, 320:626–628, May 2008. ISSN 1095-9203. doi: 10.1126/science.1148028. URL `http://www.ncbi.nlm.nih.gov/pubmed/18451293`.

David Gubbins, Ashley P Willis, and Binod Sreenivasan. Correlation of Earth's magnetic field with lower mantle thermal and seismic structure. *Phys. Earth Planet. Int.*, 162:256–260, 2007. doi: 10.1016/j.pepi.2007.04.014.

Stanley R Hart. A large-scale isotope anomaly in the Southern Hemisphere mantle. *Nature*, 309: 753–757, 1984.

Yumei He and Lianxing Wen. Structural features and shear-velocity structure of the Pacific Anomaly. *J. Geophys. Res.*, 114:1–17, 2009. doi: 10.1029/2008JB005814.

Yumei He and Lianxing Wen. Geographic boundary of the Pacific Anomaly and its geometry and transitional structure in the north. *J. Geophys. Res.*, 117(B9): 1–16, September 2012. ISSN 0148-0227. doi: 10.1029/2012JB009436. URL `http://www.agu.org/pubs/crossref/2012/2012JB009436.shtml`.

Michael A H Hedlin and Peter M Shearer. An analysis of large-scale variations in small-scale mantle heterogeneity using Global Seismographic Network recordings of precursors to PKP. *J. Geophys. Res.*, 105(B6):13655–13673, 2000.

Don V Helmberger and Sidao Ni. Seismic Modeling Constraints on the South African Super Plume. In *Earth's Deep Mantle: Structure, Composition, and Evolution*, pages 63–81. American Geophysical Union, 2005.

Don V. Helmberger, T. Lay, Sidao Ni, Michael Gurnis, and Russell J Hemley. Deep Mantle Structure and the Postperovskite Phase Transition. *Proceedings of the National Academy of Sciences of the United States of America*, 102:17257–17263, 2005.

Don V. Helmberger, Daoyuan Sun, Lijun Liu, Eh Tan, and Michael Gurnis. Review of large low shear velocity provinces in the lower mantle. *Geochimica et Cosmochimica Acta*, 73:520, 2009.

Alexander R Hutko, Thorne Lay, Edward J Garnero, and Justin Revenaugh. Seismic detection of folded, subducted lithosphere at the core-mantle boundary. *Nature*, 441:333–6, May 2006. ISSN 1476-4687. doi: 10.1038/nature04757. URL `http://www.ncbi.nlm.nih.gov/pubmed/16710418`.

Alexander R. Hutko, Thorne Lay, and Justin Revenaugh. Localized double-array stacking analysis of PcP: D and ULVZ structure beneath the Cocos plate, Mexico, central Pacific, and north Pacific. *Phys. Earth Planet. Int.*, 173:60–74, March 2009. ISSN 00319201. doi: 10.1016/j.pepi.2008.11.003. URL `http://linkinghub.elsevier.com/retrieve/pii/S0031920108003452`.

Miaki Ishii and Jeroen Tromp. Normal-Mode and Free-Air Gravity Constraints on Lateral Variations in Velocity and Density of Earth's Mantle. *Science*, 285:1231–1236, August 1999. ISSN 00368075. doi: 10.1126/science.285.5431.1231. URL `http://www.sciencemag.org/cgi/doi/10.1126/science.285.5431.1231`.

S I Karato. *The Dynamic Structure of the Deep Earth: An Interdisciplinary Approach*. Princeton University Press, Princeton, NJ, 2003.

B L N Kennett and E R Engdahl. Traveltimes for global earthquake location and phase identification. *Geophys. J. Int.*, 105:429–465, 1991.

S Labrosse, J W Hernlund, and N Coltice. A crystallizing dense magma ocean at the base of the Earth's mantle. *Nature*, 450:4–7, 2007. doi: 10.1038/nature06355.

G Laske, G Masters, Z Ma, and M E Pasyanos. CRUST1.0: An Updated Global Model of Earth's Crust. *Geophysical Research Abstracts*, 14, 2012.

Thorne Lay and Edward J Garnero. Deep Mantle Seismic Modeling and Imaging. *Ann. Rev. Earth planet. Sci.*, 39:91–123, 2011. doi: 10.1146/annurev-earth-040610-133354.

Thorne Lay, John Hernlund, Edward J Garnero, and Michael S Thorne. A post-perovskite lens and D" heat flux beneath the central Pacific. *Science*, 314:1272–6, November 2006. ISSN 1095-9203. doi: 10.1126/science.1133280. URL `http://www.ncbi.nlm.nih.gov/pubmed/17124317`.

Vedran Lekic, Sanne Cottaar, Adam Dziewonski, and Barbara Romanowicz. Cluster analysis of global lower mantle tomography: A new class of structure and implications for chemical heterogeneity. *Earth and Planetary Science Letters*, 357-358: 68–77, December 2012. ISSN 0012821X. doi: 10.1016/j.epsl.2012.09.014. URL `http://linkinghub.elsevier.com/retrieve/pii/S0012821X12005109`.

Mingming Li and Allen K McNamara. The difficulty for subducted oceanic crust to accumulate at the Earth's core-mantle boundary. *J. Geophys. Res.*, 118:1807–1816, 2013. doi: 10.1002/jgrb.50156.

Sheng-Nian Luo, Sidao Ni, and Donald V. Helmberger. Evidence for a sharp lateral variation of velocity at the coremantle boundary from multipathed PKPab. *Earth Planet. Sci. Lett.*, 189:155–164, July 2001. ISSN 0012821X. doi: 10.1016/S0012-821X(01)00364-8. URL `http://linkinghub.elsevier.com/retrieve/pii/S0012821X01003648`.

Henk Marquering, Guust Nolet, and F.a. Dahlen. Three-dimensional waveform sensitivity kernels. *Geophysical Journal International*, 132(3):521–534, March 1998. ISSN 0956540X. doi: 10.1046/j.1365-246X.1998.00426.x. URL `http://doi.wiley.com/10.1046/j.1365-246X.1998.00426.x`.

Henk Marquering, F A Dahlen, and Guust Nolet. Three-dimensional sensitivity kernels for finite-frequency traveltimes: the banana-doughnut paradox. *Geophys. J. Int.*, 137:805–815, 1999.

Guy Masters, Gabi Laske, Harold Bolton, and Adam Dziewonski. The Relative Behaviour of Shear Velocity, Bulk Sound Speed, and Compressional Velocity in the Mantle: Implications for Chemical and Thermal Structure. In *Earth's Deep Interior: Mineral Physics and Tomography from the Atomic to the Global Scale, Geophysical Monograph 117*, pages 63–87. American Geophysical Union, 2000.

Allen K McNamara and Shijie Zhong. Thermochemical structures beneath Africa and the Pacific Ocean. *Nature*, 437:1136–9, October 2005. ISSN 1476-4687. doi: 10.1038/nature04066. URL `http://www.ncbi.nlm.nih.gov/pubmed/16237440`.

Allen K. McNamara, Edward J. Garnero, and Sebastian Rost. Tracking deep mantle reservoirs with ultra-low velocity zones. *Earth Planet. Sci. Lett.*, 299: 1–9, October 2010. ISSN 0012821X. doi: 10.1016/j.epsl.2010.07.042. URL `http://linkinghub.elsevier.com/retrieve/pii/S0012821X10004802`.

Anne S. Meltzer, Roberta Rudnick, Peter Zeitler, Alan Levander, Gene Humpheys, Karl Karlstrom, Göran Ekström, R.W. Carlson, Tim Dixon, Michael Gurnis, Peter Shearer, and Robert D. van der Hilst. USArray Initiative. *GSA Today*, pages 8–10, 1999.

I. Mosca, L. Cobden, A. Deuss, J. Ritsema, and J. Trampert. Seismic and mineralogical structures of the lower mantle from probabilistic tomography. *Journal of Geophysical Research*, 117(B6):B06304, June 2012. ISSN 0148-0227. doi: 10.1029/2011JB008851. URL `http://doi.wiley.com/10.1029/2011JB008851`.

Motohiko Murakami, Kei Hirose, Katsuyuki Kawamura, Nagayoshi Sata, and Yasuo Ohishi. Post-perovskite phase transition in MgSiO3. *Science*, 304:855–8, May 2004. ISSN 1095-9203. doi: 10.1126/science.1095932. URL http://www.ncbi.nlm.nih.gov/pubmed/15073323.

Sidao Ni and Don V Helmberger. Seismological constraints on the South African superplume; could be the oldest distinct structure on earth. *Earth Planet. Sci. Lett.*, 206:119–131, 2003a.

Sidao Ni and Don V Helmberger. Ridge-like lower mantle structure beneath South Africa. *J. Geophys. Res.*, 108:1–14, 2003b. ISSN 0148-0227. doi: 10.1029/2001JB001545. URL http://www.agu.org/pubs/crossref/2003/2001JB001545.shtml.

Sidao Ni, Eh Tan, Michael Gurnis, and Don Helmberger. Sharp sides to the African superplume. *Science*, 296:1850–1852, June 2002. ISSN 1095-9203. doi: 10.1126/science.1070698. URL http://www.ncbi.nlm.nih.gov/pubmed/12052955.

Artem R Oganov and Shigeaki Ono. Theoretical and experimental evidence for a post-perovskite phase of MgSiO3 in Earth's D" layer. *Nature*, 430:445–448, 2004.

Mark Panning and Barbara Romanowicz. A three-dimensional radially anisotropic model of shear velocity in the whole mantle. *Geophysical Journal International*, 167(1):361–379, October 2006. ISSN 0956540X. doi: 10.1111/j.1365-246X.2006.03100.x. URL http://gji.oxfordjournals.org/cgi/doi/10.1111/j.1365-246X.2006.03100.x.

N. Rawlinson and B. L. N. Kennett. Rapid estimation of relative and absolute delay times across a network by adaptive stacking. *Geophysical Journal International*, 157(1): 332–340, April 2004. ISSN 0956540X. doi: 10.1111/j.1365-246X.2004.02188.x. URL http://gji.oxfordjournals.org/cgi/doi/10.1111/j.1365-246X.2004.02188.x.

M. A. Richards, Yanick Ricard, Carolina Lithgow-Bertelloni, Giorgio Spada, and Roberto Sabadini. An Explanation for Earth's Long-Term Rotational Stability. *Science*, 275 (5298):372–375, January 1997. ISSN 00368075. doi: 10.1126/science.275.5298.372. URL http://www.sciencemag.org/cgi/doi/10.1126/science.275.5298.372.

Mark A Richards and David C Engebretson. Large-scale mantle convection and the history of subduction. *Letters to Nature*, 355:437–440, 1992.

J. Ritsema, H. J. van Heijst, and John H. Woodhouse. Complex Shear Wave Velocity Structure Imaged Beneath Africa and Iceland. *Science*, 286(5446):1925–1928, December 1999. ISSN 00368075. doi: 10.1126/science.286.5446.1925. URL http://www.sciencemag.org/cgi/doi/10.1126/science.286.5446.1925.

J. Ritsema, A. Deuss, H. J. van Heijst, and J. H. Woodhouse. S40RTS: a degree-40 shear-velocity model for the mantle from new Rayleigh wave dispersion, teleseismic traveltime and normal-mode splitting function measurements. *Geophysical Journal International*, 184 (3):1223–1236, March 2011. ISSN 0956540X. doi: 10.1111/j.1365-246X.2010.04884.x. URL http://gji.oxfordjournals.org/cgi/doi/10.1111/j.1365-246X.2010.04884.x.

Jeroen Ritsema, Edward J. Garnero, and Thorne Lay. A strongly negative shear velocity gradient and lateral variability in the lowermost mantle beneath the Pacific. *J. Geophys. Res.*, 102:20,395–20,411, 1997.

Jeroen Ritsema, Sidao Ni, Donald V Helmberger, and H Philip Crotwell. Evidence for strong shear velocity reductions and velocity gradients in the lower mantle beneath Africa. *Geophys. Res. Lett.*, 25:4245–4248, 1998.

G S Robertson and J H Woodhouse. Constraints on lower mantle physical properties from seismology and mineral physics. *Earth Planet. Sci. Lett.*, 143:197–205, 1996a.

G S Robertson and J. H. Woodhouse. Ratio of relative S to P velocity heterogeneity in the lower mantle. *J. Geophys. Res.*, 101:20,041–20,052, 1996b.

Sebastian Rost and Edward J. Garnero. A study of the uppermost inner core from PKKP and PP differential traveltimes. *Geophys. J. Int.*, 156:565–574, March 2004. ISSN 0956540X. doi: 10.1111/j.1365-246X.2004.02139.x. URL http://doi.wiley.com/10.1111/j.1365-246X.2004.02139.x.

Sebastian Rost and Edward J. Garnero. Detection of an ultralow velocity zone at the core-mantle boundary using diffracted PKKP ab waves. *J. Geophys. Res.*, 111:1–8, 2006. ISSN 0148-0227. doi: 10.1029/2005JB003850. URL http://www.agu.org/pubs/crossref/2006/2005JB003850.shtml.

Sebastian Rost, Edward J Garnero, Quentin Williams, and Michael Manga. Seismological constraints on a possible plume root at the core-mantle boundary. *Nature*, 435:666–9, June 2005. ISSN 1476-4687. doi: 10.1038/nature03620. URL http://www.ncbi.nlm.nih.gov/pubmed/15931220.

Haruo Sato and Michael C Fehler. *Seismic Wave Propogation and Scattering in the Heterogeneous Earth*. Springer Verlag and AIP Press, New York, 2nd edition, 2008.

B. S. A. Schuberth, H.-P. Bunge, and J. Ritsema. Tomographic filtering of high-resolution mantle circulation models: Can seismic heterogeneity be explained by temperature alone? *Geochem. Geophys. Geosyst.*, 10, May 2009. ISSN 1525-2027. doi: 10.1029/2009GC002401. URL http://www.agu.org/pubs/crossref/2009/2009GC002401.shtml.

Nathan A. Simmons, Alessandro M. Forte, Lapo Boschi, and Stephen P. Grand. GyPSuM: A joint tomographic model of mantle density and seismic wave speeds. *Journal of Geophysical Research*, 115(B12):B12310, December 2010. ISSN 0148-0227. doi: 10.1029/2010JB007631. URL http://doi.wiley.com/10.1029/2010JB007631.

Bernhard Steinberger and Trond H Torsvik. Absolute plate motions and true polar wander in the absence of hotspot tracks. *Nature*, 452(7187):620–3, April 2008. ISSN 1476-4687. doi: 10.1038/nature06824. URL http://www.ncbi.nlm.nih.gov/pubmed/18385737.

Xinlei Sun, Xiaodong Song, Sihua Zheng, and Don V Helmberger. Evidence for a chemical-thermal structure at base of mantle from sharp lateral P-wave variations beneath Central America. *Proceedings of the National Academy of Sciences of the United States of America*, 104:26–30, 2007.

Eh Tan and Michael Gurnis. Metastable superplumes and mantle compressibility. *Geophys. Res. Lett.*, 32:1–4, 2005. ISSN 0094-8276. doi: 10.1029/2005GL024190. URL http://www.agu.org/pubs/crossref/2005/2005GL024190.shtml.

Eh Tan and Michael Gurnis. Compressible thermochemical convection and application to lower mantle structures. *Journal of Geophysical Research*, 112(B6):B06304, June 2007. ISSN 0148-0227. doi: 10.1029/2006JB004505. URL http://doi.wiley.com/10.1029/2006JB004505.

Christine Thomas, Edward J. Garnero, and Thorne Lay. High-resolution imaging of lowermost mantle structure under the Cocos plate. *J. Geophys. Res.*, 109:1–11, 2004. ISSN 0148-0227. doi: 10.1029/2004JB003013. URL http://www.agu.org/pubs/crossref/2004/2004JB003013.shtml.

M Thorne, Edward J. Garnero, and Stephen P. Grand. Geographic correlation between hot spots and deep mantle lateral shear-wave velocity gradients. *Phys. Earth Planet. Int.*, 146:47–63, August 2004. ISSN 00319201. doi: 10.1016/j.pepi.2003.09.026. URL `http://linkinghub.elsevier.com/retrieve/pii/S003192010400113X`.

Michael S. Thorne, Thorne Lay, Edward J. Garnero, Gunnar Jahnke, and Heiner Igel. Seismic imaging of the laterally varying D region beneath the Cocos Plate. *Geophys. J. Int.*, 170:635–648, August 2007. ISSN 0956540X. doi: 10.1111/j.1365-246X.2006.03279.x. URL `http://doi.wiley.com/10.1111/j.1365-246X.2006.03279.x`.

Michael S. Thorne, Edward J. Garnero, Gunnar Jahnke, Heiner Igel, and Allen K. McNamara. Mega ultra low velocity zone and mantle flow. *Earth and Planetary Science Letters*, 364:59–67, February 2013a. ISSN 0012821X. doi: 10.1016/j.epsl.2012.12.034. URL `http://linkinghub.elsevier.com/retrieve/pii/S0012821X12007200`.

Michael S. Thorne, Yang Zhang, and Jeroen Ritsema. Evaluation of 1-D and 3-D seismic models of the Pacific lower mantle with S, SKS, and SKKS traveltimes and amplitudes. *Journal of Geophysical Research: Solid Earth*, 118(3):985–995, March 2013b. ISSN 21699313. doi: 10.1002/jgrb.50054. URL `http://doi.wiley.com/10.1002/jgrb.50054`.

A To, B Romanowicz, Y Capdeville, and N Takeuchi. 3D effects of sharp boundaries at the borders of the African and Pacific Superplumes: Observation and modeling. *Earth planet. Sci. Lett.*, 233:137–153, April 2005. ISSN 0012821X. doi: 10.1016/j.epsl.2005.01.037. URL `http://linkinghub.elsevier.com/retrieve/pii/S0012821X05001007`.

Trond H. Torsvik, Mark A. Smethurst, Kevin Burke, and Bernhard Steinberger. Large igneous provinces generated from the margins of the large low-velocity provinces in the deep mantle. *Geophys. J. Int.*, 167:1447–1460, December 2006. ISSN 0956540X. doi: 10.1111/j.1365-246X.2006.03158.x. URL `http://doi.wiley.com/10.1111/j.1365-246X.2006.03158.x`.

Jeannot Trampert, Frédéric Deschamps, Joseph Resovsky, and Dave Yuen. Probabilistic tomography maps chemical heterogeneities throughout the lower mantle. *Science*, 306:853–6, October 2004. ISSN 1095-9203. doi: 10.1126/science.1101996. URL `http://www.ncbi.nlm.nih.gov/pubmed/15514153`.

Reidar G. Trønnes. Structure, mineralogy and dynamics of the lowermost mantle. *Miner. Petrol.*, 99:243–261, July 2010. ISSN 0930-0708. doi: 10.1007/s00710-009-0068-z. URL `http://www.springerlink.com/index/10.1007/s00710-009-0068-z`.

Peter E. van Keken, Erik H. Hauri, J. P. Brandenburg, and Chris J. Ballentine. Generation of mantle heterogeneity by ocean crust recycling: Geophysical and geochemical constraints. *Geochimica et Cosmochimica Acta*, 74:1072, 2010.

Yi Wang and Lianxing Wen. Mapping the geometry and geographic distribution of a very low velocity province at the base of the Earth's mantle. *J. Geophys. Res.*, 109(B10):B10305, 2004. ISSN 0148-0227. doi: 10.1029/2003JB002674. URL `http://www.agu.org/pubs/crossref/2004/2003JB002674.shtml`.

Yi Wang and Lianxing Wen. Geometry and P and S velocity structure of the African Anomaly. *J. Geophys. Res.*, 112:1–26, May 2007. ISSN 0148-0227. doi: 10.1029/2006JB004483. URL `http://www.agu.org/pubs/crossref/2007/2006JB004483.shtml`.

Lianxing Wen. Seismic evidence for a rapidly varying compositional anomaly at the base of the Earths mantle beneath the Indian Ocean. *Earth Planet. Sci. Lett.*, 194: 83–95, December 2001. ISSN 0012821X. doi: 10.1016/S0012-821X(01)00550-7. URL `http://linkinghub.elsevier.com/retrieve/pii/S0012821X01005507`.

Lianxing Wen, Paul Silver, David James, and Randy Kuehnel. Seismic evidence for a thermo-chemical boundary at the base of the Earths mantle. *Earth Planet. Sci. Lett.*, 189:141–153, July 2001. ISSN 0012821X. doi: 10.1016/S0012-821X(01)00365-X. URL `http://linkinghub.elsevier.com/retrieve/pii/S0012821X0100365X`.

Q. Williams, J. Revenaugh, and E. J. Garnero. A Correlation Between Ultra-Low Basal Velocities in the Mantle and Hot Spots. *Science*, 281:546–549, July 1998. doi: 10.1126/science.281.5376.546. URL `http://www.sciencemag.org/cgi/doi/10.1126/science.281.5376.546`.

Michael E Wysession, Amy Langenhorst, Matthew J Fouch, Karen M Fischer, Ghassan I Al-eqabi, Patrick J Shore, and Timothy J Clarke. Lateral Variations in Compressional / Shear Velocities at the Base of the Mantle. *Science*, 284:120–125, 1999.

Highlights

- P-wave travel-time deviations caused by the Pacific LLSVP are detected at USArray
- We create the first high-resolution map of the LLSVP edge detected with P-waves
- LLSVP boundary is seismically diffuse in the central Pacific, and sharp in the east
- The edge shape and sharpness may be linked with dynamics and subduction history
- P-wave LLSVP boundary roughly matches the S-wave boundary, except at the eastern edge